Geomorphology on geologic timescales: Evolution of the late Cenozoic Pacific paleosurface in Northern Chile and Southern Peru

L.A. Evenstar, A.E. Mather, A.J. Hartley, F.M. Stuart, R.S.J. Sparks, F.J. Cooper

PII: S0012-8252(16)30205-7
DOI: doi: 10.1016/j.earscirev.2017.04.004
Reference: EARTH 2403

To appear in: *Earth-Science Reviews*

Received date: 26 July 2016
Revised date: 5 April 2017
Accepted date: 7 April 2017
Embargo release date: 7th April 2018

Please cite this article as: L.A. Evenstar, A.E. Mather, A.J. Hartley, F.M. Stuart, R.S.J. Sparks, F.J. Cooper , Geomorphology on geologic timescales: Evolution of the late Cenozoic Pacific paleosurface in Northern Chile and Southern Peru. The address for the corresponding author was captured as affiliation for all authors. Please check if appropriate. Earth(2017), doi: 10.1016/j.earscirev.2017.04.004

GEOMORPHOLOGY ON GEOLOGIC TIMESCALES: EVOLUTION OF THE LATE CENOZOIC PACIFIC PALEOSURFACE IN NORTHERN CHILE AND SOUTHERN PERU

L.A. Evenstar*[1], A.E. Mather[2], A.J. Hartley[3], F.M. Stuart[4], R.S.J. Sparks[1] and F.J. Cooper[1]

[1]School of Earth Sciences, University of Bristol, UK,
[2]Department of Geography, Earth and Environmental Sciences, University of Plymouth, UK,
[3]Deptartment of Geology and Petroleum Geology, University of Aberdeen, Aberdeen, UK,
[4]Isotope Geoscience Unit, Scottish Universities Environmental Research Centre, East Kilbride, UK.

Abstract

The Atacama Desert on the western margin of the Central Andes is one of the driest and oldest deserts in the world. It is defined by a distinct and ancient surface, known as the Pacific Paleosurface (PPS) or Atacama Paleosurface. The age of this surface is determined as the time at which sediment deposition ceased, and the surface was effectively abandoned. Early studies suggested that this abandonment took place between 14 and 10 Ma, and was related to both the uplift of the Andes and the onset of hyperaridity in the region. Here we provide a regional re-examination of the PPS, compiling existing work on the underlying geology, sedimentology, surface exposure dating, and seismic profiling. We also present new multispectral satellite maps of the PPS and 45 new cosmogenic ^{3}He and ^{21}Ne surface exposure ages in order to constrain the formation age, and the preservation and incision history of the paleosurface. We conclude that the PPS is not a single paleosurface, but instead is a mosaic of smaller surfaces that were formed by aggradational and degradational processes over 19 million years (or more) and should be termed collectively as the Pacific Paleosurfaces. The time at which individual paleosurfaces formed is related to regional climate, where the location of each is controlled by regional tectonic activity. Cosmogenic surface exposure ages suggest that the surfaces are a record of regional scale climate events.

Keywords; *Andes; Pediment; Paleosurface; cosmogenic surface exposure dating; Atacama; Desert Pavement; landscape evolution; climate; tectonics; remote sensing*

1. Introduction

The Pacific Paleosurface (PPS) stretches for over 1,200 km along the western margin of the Central Andes in northern Chile and southern Peru (Evenstar et al. 2009). Previous names include the Atacama Pediplain (e.g. Galli-Oliver 1967), El Diablo-Altos de Pica Paleosurface (Hoke et al. 2007) and Atacama Bench (Armijo et al. 2010). It is located between the Coastal Cordillera to the west and Andean Precordillera and Western Cordillera to the east (Fig 1a). It is 50 to 70 km wide, it has an average westward tilt of 3-4°, and is approximately coincident with the top of the Longitudinal Valley. For decades it has been believed to be largely erosional in origin (Segerstrom, 1963) but is locally covered by Middle Miocene age alluvial gravels, termed the "Atacama gravels" (Mortimer, 1973). In northern Chile, the surface is incised by ≤1,700 m-deep rivers ('quebradas') that flow west from the Andes to the Pacific Ocean.

The exceptional preservation of the PPS is a result of the long-lived regional presistent arid climate, and provides a unique opportunity to examine the development of regionally extensive geomorphic surfaces over geologic time-scales at a classic destructive plate margin. By understanding how and when the PPS formed and how it has evolved, we can place new constraints on how tectonic processes and climate change have shaped the modern landscape of the Central Andes. The PPS is also of economic interest since supergene enrichment of porphyry copper deposits ceased across the region during its development (e.g. Segerstorm 1963, Hollingworth 1964, Hartley and Rice 2005). This implies that the controls on these two events may be related.

The formation of a paleosurface can occur by two mechanisms; cessation of active deposition on a surface, or the end of active erosion. In both cases, the surface is "abandoned" and only undergoes superficial modification. The time at which the PPS formed is debated. A widely held view is that the entire PPS formed and was incised

during a relatively narrow time interval between 14 Ma and 10 Ma, triggered either by a regional increase in aridity or rapid uplift of the Andes (e.g. Galli-Oliver 1967, Tosdal et al. 1984, Alpers and Brimhall 1988, Farías et al. 2005, Hoke et al. 2007). More recently, the PPS has been interpreted as a composite paleosurface that developed from the Miocene (Evenstar et al. 2009) to the Pleistocene (Jordan et al. 2014).

The lack of good chronological constraints reflects the fact that previous studies have concentrated on relatively small sections of the PPS (e.g. Quang et al. 2005, Evenstar et al. 2009, Jordan et al. 2014). Here we present a synoptic view of the entire surface. We combine regional multispectral satellite mapping and field observations to constrain the spatial extent and internal complexity of the PPS with new cosmogenic ^{3}He and ^{21}Ne surface exposure ages of four key surfaces within it. Our results are integrated with previously-published surface exposure ages, sediment analyses and seismic studies to demonstrate that the PPS formed diachronously from the start of the Miocene to the Pleistocene. The observations allow us to reconstruct the evolution of this complex landscape and use it to infer how both tectonic and climatic processes have interacted along the western margin of the Central Andes and how these processes vary from north to south along the Longitudinal Valley (Figure 1A).

2. Geological Setting

2.1 Morphotectonic provinces

The Central Andes can be divided into five main morphotectonic provinces. From west to east these are the: Coastal Cordillera, Longitudinal Valley, Precordillera, Western Cordillera, Altiplano, and Eastern Cordillera (Figure 1A).

The Coastal Cordillera rises abruptly from the Pacific Ocean to reach over 3,000 m in elevation, with a maximum width of 60 km near the Rio Loa (22°S; Figure 1A). The elevation and width of the range decreases northwards until it disappears completely at the Bolivian Orocline (18°30'S; Figure 1A), before reappearing again at

18°15'S in southern Peru, where it increases in elevation and width northwards. The Coastal Cordillera is a Jurassic-Early Cretaceous magmatic arc dissected by a series of faults (Allmendinger et al. 2005). Following a period of extension in the Early Cretaceous, the extensional basins are infilled with Late Oligocene to Early Miocene volcaniclastic sediments (Coira et al. 1982). During the Late Oligocene, large-scale sedimentation ceased within the Coastal Cordillera forming a relict paleosurface termed the Coastal Tarapaca Pediplain (Mortimer and Saric 1972) (Figure 1B).

To the east of the Coastal Cordillera lies the Longitudinal Valley (also referred to as the Pampas del Tamarugal or Central Basin/Central Depression in northern Chile, and the Llanuras Costaneras in southern Peru), a deep forearc basin. For simplicity, we refer to the entire region from northern Chile to southern Peru as the Longitudinal Valley. Along its length, the basin varies in width from 30 to 70 km and at the Bolivian Orocline, where the Coastal Cordillera is absent it ranges in elevation from sea level to 2,000 m on its eastern margin. To the north and south of the Bolivian Orocline, the elevation of the basin gradually increases.

The Longtitudinal Valley is infilled with up to 1500 m of Eocene to Pliocene age sedimentary deposits that originate from the Precordillera to the east (Mortimer and Redic, 1975, Hartley et al. 2000, Hartley and Evenstar, 2010, Jordan et al. 2015). It is thought that the PPS formed when sediment deposition ceased, which we will show *a posteriori* occurred in pulses and ceased diachronously across the surface and, in some places, began in the early Miocene. South of 19°30'S, the PPS is internally drained whereas to the north, in northern Chile, five deep canyons (the Lluta, Azapa, Victor, Camarones and Tana Quebradas) incise up to 1,700 m into the surface and drain to the Pacific Ocean. Similarly, in southern Peru, five ≤1,500 m-deep canyons cut across the PPS and drain to the Pacific Ocean: the Rio Tambo, Rio Sama, Rio Moquegua, Rio Locumba, and Rio Caplina (Figure 2A). The Atacama Fault system forms a prominent boundary over 1000 km in length (21–26ºS) between the Coastal Cordillera and the Longitudinal Valley.

To the east of the Longitudinal Valley, the Precordillera reaches a maximum elevation of 4,000 m and varies in width from 10 to 70 km (Hartley et al. 2000). The range is composed of Late Cretaceous to Oligocene magmatic and volcanic rocks (Charrier et al. 2012) covered in large parts by Miocene ignimbrites that have been locally deformed into large wavelength anticlines and monoclines (Garcia and Hérail, 2005; van Zalninge et al. 2016). South of 22°S, the Precordillera decreases in elevation to 3000 m and is defined by a series of large disconnected Cenozoic foreland basins termed the Pre-Andean Basins (Figure 1A). At 22°30'S, the Rio Loa cuts through one of these basins, the Calama Basin, en route to the Pacific Ocean (Figure 2A).

On the eastern margin of the Precordillera, the 50–100 km-wide Western Cordillera houses a foreland fold and thrust belt and the modern volcanic arc, with volcanic peaks up to 6,000 m high. Between the Western Cordillera and Eastern Cordillera lies the Altiplano, a ca. 200 km-wide, 3,800 m-high internally drained basin infilled with Neogene to recent sedimentary and volcanic deposits (Lamb et al. 1997).

Andean orogenesis commenced in the Jurassic with the subduction of oceanic lithosphere beneath the eastern margin of South America (Jordan et al. 1983). Initially, the magmatic arc was located within the Coastal Cordillera but has since migrated progressively eastward, reaching its current location in the Western Cordillera in the mid late Miocene. The region now occupied by the Altiplano initially formed as a backarc basin (Allmendinger et al. 1997) but since the Late Cretaceous, it has been uplifted and now forms an internally drained basin sandwiched between the Western and Eastern Cordillera. The Eastern Cordillera has been an area of active uplift since the Late Cretaceous, but deformation likely ceased in the mid to late Miocene when active tectonic shortening was displaced to the east (Kennan et al. 1995).

At the Chile-Peru border (18°S), the Bolivian Orocline represents a bend in the Andean mountain chain, which is thought to have existed since Eocene to Oligocene time (Arriagada et al. 2008). The origin of the orocline is poorly constrained, with

current theories ranging from enhancement of an original concave structure by differential plate shortening along strike (Isacks 1988) to variation in the thickness of the downgoing slab (Capitanio et al. 2011).

The timing of Andean uplift is also controversial (e.g. Barnes and Ehlers 2009 and references therein), with two main schools of thought. One theory prerdicts rapid late Miocene surface uplift of ~2.5 km within the Altiplano between 11 and 6 Ma due to large-scale mantle delamination of the continental lithosphere (Garzione et al. 2006; Ghosh et al. 2006, Molnar and Garzione 2007; Garzione et al. 2008; Hoke and Garzione 2008, Farías et al. 2005). A second model sees slow and steady uplift from the late Eocene onwards, associated with crustal shortening and thickening in response to oblique subduction of the Nazca plate (Victor et al. 2004; Barke and Lamb, 2006; Hartley et al., 2007; Barnes and Ehlers, 2009; Juez-Parré et al., 2010; Evenstar et al. 2015b, Lamb 2016).

2.2 Formation of the Pacific Paleosurface

Within this tectonic framework, the Pacific Paleosurface formed over an area of ca. 60,000 km^2. The time of "formation" is defined as the time at which large-scale active deposition or erosion of the surface ceased, and it was effectively "abandoned". Thus surfaces within the PPS are defined as either: (1) degradational, whereby the top of the surface is characterised by erosive features (Garcia and Hérial 2005), or (2) aggradational, whereby the top of the surface is characterised by sedimentary deposits (Segerstorm 1963; Galli-Oliver 1967; Mortimer et al. 1974; Tosdal et al. 1984; Quang et al. 2005; Farías et al. 2005; Hoke et al. 2007).

Within the Longitudinal Valley these processes are governed by ephemeral fluvial systems. Whether these fluvial systems are in net aggradation or net degradation (incision) is largely dependent on the balance between bottom up processes such as base level controls and top down processes, such as climate, which drive sediment supply (e.g. Schumm et al. 1993; Mather et al. 2016 and references therein). Any changes in either climate or tectonics can drive geomorphic instabilities, shifting the location of aggradation and deposition within the fluvial systems. The PPS has long

been regarded as forming in a narrow period of time due to either a shift in the climate to hyperarid in the mid-Miocene reducing erosion and deposition of sediments (Galli-Oliver 1967, Mortimer and Rendic 1975, Alpers and Brimhall 1988) or due to rapid uplift of the Andes increasing the steepness of the river profiles to the east, leading to incision of the fluvial systems in the same region (Tosdal et al. 1984; Farías et al. 2005; Hoke et al. 2007; Garzione et al. 2008). These alternatives are not mutually exclusive. However, as will be demonstrated below, the PPS is an amalgamation of several individual paleosurfaces, formed over a much longer time than many of these studies propose.

3. Methods

In order to constrain the age of the PPS across northern Chile and southern Peru, we combined a number of different observations and strands of evidence from previous studies and our own data, as follows:

1. Stratigraphic and paleosurface studies were combined with new field observations from the Longitudinal Valley and integrated with East-West seismic reflection profiles and field transects to: a) constrain the timing and regional distribution of sediments, b) constrain the evolution of the landscape and accommodation space, and c) infer how sediment supply has been influenced by uplift of the Andes and regional changes in climate.
2. Multispectral satellite data and digital elevation models (DEMs) were combined to map the spatial extent and internal complexity of the PPS based on morphological and compositional characteristics.
3. Elevation profiles were constructed from the DEM data throughout the Longitudinal Valley and along modern river systems to constrain their relative timing of incision into the PPS.
4. New cosmogenic surface exposure ages were obtained for 45 boulders collected from several surfaces in northern Chile. These ages, together with previously published surface exposure ages are used to constrain the temporal evolution of the PPS.

3.1 Sediments and Seismic Reflection Profiles

Most sedimentological studies of northern Chile and southern Peru have focused on small regions or single basins (e.g. Victor et al., 2004; Pinto et al., 2004; Farías et al., 2005). However, a few studies in northern Chile have evaluated how the smaller-scale sedimentology can be linked across the region (Hartley et al., 2000; Hartley and Evenstar, 2010; Jordan et al., 2014). Here we review sedimentological studies from southern Peru at 16°S to the Pre-Andean Depression at 23°S (Kött et al., 1995; Sáez et al., 1999, 2012; Gaupp et al., 1999; May et al., 1999, 2005, Hartley et al. 2000; Victor et al., 2004; Pinto et al., 2004; Farías et al., 2005, Quang et al., 2005, García and Hérail 2005, Roperch et al. 2006; Thouret et al., 2007; Decou et al., 2011; Evenstar et al., 2015a, Jordan et al., 2015, Alván et al., 2015) in order to construct a comprehensive chronostratigraphic chart that identifies when and where the main phases of sediment accumulation took place.

In order to constrain the east-west distribution of the sediments within the Longitudinal Valley, transects were constructed at 18°20'S, 19°20'S, and 20°45'S (Figures 1B and 3). The 19°20'S and 20°45'S transects are taken from seismic reflection studies presented in Jordan et al. (2010), but the 19°20'S transect is modified in the west after our own field observations along Quebrada Camarones (Figure 4H). Jordan et al. (2010) defined four stratigraphic units within these sections dated at 7-3.5 Ma, 14-10 Ma, 20–16 Ma and 30–20 Ma. Section 18°20'S was constructed from field observations along the Peru-Chile border and along Quebrada Lluta. In this paper, we define two additional stratigraphic units, which are integrated into the seismic sections based on field observations and previous sedimentological studies (Figure 3). The relationship between the units defined by Jordan et al. (2010) and the sedimentary sections in the regions to the north are discussed in more detail in the results.

3.2 Regional mapping of the Pacific Paleosurface

The PPS is typically characterised by a desert pavement that develops following the end of major sedimentary deposition or erosion (Evenstar et al. 2009). Desert pavements comprise a closely packed mosaic of angular pebble to cobble sized rock fragments and are recognised worldwide in arid and hyperarid regions (Figure 4C) (Wood et al. 2005). Several studies have documented how desert pavements develop over time and how variations in their characteristics can be used to correlate different geomorphic surfaces and to infer relative ages (Wells et al. 1987; McFadden et al. 1987, Al-Farraj and Harvey 2000, Wood et al. 2005). Here, we use four main features to characterise the surfaces using remotely-sensed satellite data, topographic analysis at a scale of 1 to 10 m, surface texture, desert varnish and the development of a soil beneath the desert pavement.

1. Depositional or erosional surface topography (surface texture on a 1-10 m scale in remotely-sensed data) initially forms with a bar and swale topography (Figure 4B), created by ephemeral fluvial channels. Over time the surface will evolve into a flat featureless desert pavement with eradication of the original depositional features due to a combination of deflation and sediment entrapment (Figure 4C, F and G) (Wood et al. 2005).

2. Texture and colour of surface material are commonly distinctive features. Initially the matrix of a surface is formed from deposition of fluvial sediment (mud or sand matrix). Depending upon the geology of the source area and the proximal or distal nature of the deposition, the resulting fluvial deposits may be dominated by fine-grained (sands and silt sized) or course-grained (>boulder-sized) particles. As the pavement matures, the surfaces form either a mosaic of pebble and cobble sized clasts (or ‘ghosts’ of shattered larger clasts) or, in the absence of clasts, deflation exposes an underlying, typically white, gypsiferous soil. In remotely-sensed datasets, these variations are manifested in distinctive colours of the desert surface (Figures 4C and G).

3. Desert varnish results from an accumulation of manganese and iron oxides on the surface (Wood et al. 2005), which form a hard rind on the outside of clasts (Figure 4D). The varnish masks the clast lithology and darkens over time (Thomas 2000). Viewed from afar, the surfaces change from lighter colours toward a homogenous red polished appearance (McFadden et al. 1987). These changes can be easily recognised in both satellite data and on the ground (Figure 4C).

4. Soils (surface roughness, 30 m scale) within the Atacama Desert develop below surface pavement clasts (Fig. 4E) due to the accumulation of salts and wind-blown dust (Jordan et al. 2014), and thicken over time (Wells et al. 1995). The rate of growth of these soils can vary spatially (Dancey et al. 2012; Figure 4) and the resultant expansion and 'heave' of the soil (Figure 4F) results in undulose surfaces on a >30 m wavelength, which can be identified within the satellite imagery as a textural roughness.

The regional extent of the PPS has only previously been mapped and characterised in detail in two different locations. In southern Peru from 17°S to 18°S, Tosdal et al. (1984) identified five distinct surfaces within the PPS (Altos de Camilaca, Pampas Lagunas, Cerro de las Chulpas, Pampa Sitana and Cerro Sagollo), ranging from Late Oligocene to Late Miocene in age. Quang et al. (2005) bracketed the age of these paleosurfaces at 24-23.8 Ma, 20-19 Ma, 13-15 Ma, 10.1-10 Ma and 7.9 Ma by dating the underlying and overlying volcanic units. In northern Chile, between 21°S and 22°S, the PPS is thought to be younger, having formed in five stages from the mid Miocene to the Holocene (Jordan et al. 2014). Paleosurfaces were mapped and their ages were constrained using dated volcanic units interbedded with the sediments. The surfaces, termed as Stages NI, NII, NIII, NIV and NV by Jordan et al. (2014), were believed to have formed at the end of relatively humid periods when the climate reverted back to hyperaridity at 11 Ma, 4.5 Ma, 3.6 Ma, 2.1 Ma and after 1 Ma.

In this study, PPS was mapped between 18°S and 22°S, linking together the two previously studied regions. Between 21°S and 22°S, mapped surfaces were partially integrated with the studies by Jordan et al. (2014) and Nester et al. (2007) whereas

north of 18°S the surfaces were integrated with the studies of Quang et al. (2005). South of 22°S, the PPS discontinues, as the Longitudinal Valley is divided into a series of small disconnected basins termed the Pre-Andean Basins (Figure 1A).

3.2.1 Remote sensing data

Remote sensing data from Google Earth (VNIR – Visible Near-Infrared) and Landsat (VNIR and SWIR – Shortwave Infrared) were used for preliminary mapping of the PPS between 17°S and 23°S. Pixel sizes ranged from 2.5 to 15 m in Google Earth and 30 m in the Landsat data. Landsat scenes were obtained from the Landsat 7 satellite (collected from August 1999 – June 2002) using the Enhanced Thematic Mapper (ETM+). Combinations of 3 SWIR bands were combined to generate the false colour image shown in Figure 5. Surfaces were mapped according to variations in colour and texture, such as the presence or absence of fluvial depositional features.

3.2.2 Digital Elevation Model

A 30 m-pixel resolution digital elevation model (DEM) was constructed from Advanced Spaceborne Thermal Emission and Reflection Radiometer (ASTER) satellite data (Data repository A). The model has a vertical accuracy of ~10 - 25 m and was used to construct a hillshade model of the area.

3.2.3 Surface slopes

The DEM was used to construct a map of surface slope in degrees calculated from the maximum change in elevation between each 30 m pixel (Data repository A).

3.2.4 Slope Directions

The DEM was used to construct a slope direction (aspect) map that illustrates the downslope direction between each pixel and its nearest neighbours (Data repository A). The values of the pixels are colour coded to highlight the direction they face. The slope maps can indicate the dominant slope direction of surfaces over a large area.

3.2.5 Field Observations

Surfaces mapped by combining the satellite data and digital elevation model were further constrained through field investigations. Observations of desert pavement properties (size and shape of clasts, soil type, soil depth, fragmentation of clasts, clast density, thickness of desert varnish) characterised each surface.

3.2.6 Recognising the surfaces

Aggradational surfaces were mapped according to differences in: (1) colour; (2) drainage patterns; (3) degree of surface roughness in the DEM; (4) slope angle; and (5) slope direction. Cross-cutting relationships between surfaces were observed both in the satellite images and in the field. The youngest sediments that cross-cut all features on the surface were mapped first, followed by the next youngest aggradational unit, which was shown to overlap all other paleosurfaces, and so on to establish a relative chronology for the PPS.

Degradational surfaces were identified by the presence of abandoned drainage networks and drainage capture points of older fluvial networks. The relative chronology of degradational surfaces was determined from elevation profiles whereby younger fluvial networks exhibit deeper incision into paleosurfaces and fewer branches to older drainage networks. Subsequent drainage networks that captured all prior drainages were then identified and mapped. This procedure was repeated for all drainage networks. Detailed maps of all surfaces that comprise the PPS are presented in supplementary material and summarised in Figure 6.

3.3 Elevation Profiles

Elevation profiles were constructed both along the length of the PPS from northern Chile to southern Peru and across it, following the quebradas that incise it (Figure 2A). In order to constrain the evolution of the PPS in regions where it is strongly eroded, remnant parts of the older paleosurface, identified as the highest aggradational surface in the region, were used to project where the paleosurface would have been prior to erosion. Throughout this region the width of the Coastal Cordillera was also measured. These data are presented in Figure 7.

Six river profiles were constructed across the Longitudinal Valley comparing the elevation of the PPS to the modern river (Figure 2). The four northernmost river profiles were taken from the externally drained part of the basin and have previously been published by Garcia et al. (2011). A further four valley cross-sections were constructed perpendicular to these river profiles close to the Coastal Cordillera (Figure 2). Elevation profiles were taken at 19°45'S and 20°55'S within the internally drained part of the Longitudinal Valley. Cross-sections were not taken on these rivers, as there is no elevation difference between the PPS and the modern drainage system proximal to the Coastal Cordillera.

3.4 Cosmogenic nuclide data

Cosmogenic nuclide analysis can constrain the exposure age of a paleosurface within a stable landscape (Dunai et al. 2004, Kober et al. 2007, Nishizumii et al. 2005, Evenstar et al. 2009). Within the Atacama desert numerous cosmogenic isotope studies have shown that boulders are the most stable part of the landscape (Placzek et al. 2010, Jungers et al. 2013 and Matmon et al. 2015). Surrounding sediments and soils are affected by aeolian, ephemeral fluvial or soil forming processes that rework smaller size clasts (Jungers te al. 2013). In order to constrain the last major fluvial event to form the paleosurface we measured cosmogenic ^{3}He and ^{21}Ne concentrations in 45 boulders of fluvial origin from 20 sites across the PPS (Figure 5). The largest boulders at each site were selected as they were deemed most likely to have avoided significant erosion, movement, and weathering since deposition. The boulders ranged in size from 25 cm to 80 cm, with the exception of samples 1-3 which were ~10 cm clasts. All boulders were located away from local topographical features so that shielding corrections were not required. Sample locations and elevations were recorded on a hand held GPS (Table 1).

The top 5 cm of each boulder was sampled, crushed and sieved to a grain size of 500–125 µm. Heavy liquids and a magnetic separator were used to isolate the appropriate mineral fractions, which were then cleaned in an ultrasonic bath in 20 %

nitric acid. Pure fractions of pyroxene, amphibole and olivine crystals were hand picked under a binocular microscope for ^{3}He determinations. For ^{21}Ne, hand picked quartz grains were crushed to < 125 µm then treated with HF. Samples of 40-80 mg were analysed using the MAP215-50 mass spectrometer at the Scottish Universities Environmental Research Centre following standard analytical procedures (Codilean et al. 2008, Foeken et al. 2009).

To calculate surface exposure ages, we used the weighted mean of the cosmogenic ^{3}He production rate in olivine compiled by Goehring et al. (2010) and incorporated recent measurements of production rate (Foeken et al., 2012; Blard et al., 2013). These measurements gave a sea level high-latitude production rate of 119.3 ± 3.0 atoms/g/year for Lal (1999) for ^{3}He. This value was then scaled for the composition of the analysed minerals using the element production rates of Masarik (2002). Amphibole samples were assumed to contain a 10% contribution of ^{3}He produced by cosmogenic thermal neutrons (CTN) on ^{6}Li based on similar samples from this location (Evenstar et al. 2015b). The sea level high-latitude production rate of ^{21}Ne in quartz was assumed to be 18.3 ± 3.0 atoms/g/year (Balco and Shuster, 2009). The scaling factors of Lal (1991) modified by Stone (2000) (‘*lm’* (Balco et al. 2008)) were used as these have been established as more accurate than the neutron monitor based scaling schemes (Lifton et al. 2014). The regional uplift of the region has varied over the apparent exposure time of the samples. An early Miocene uplift history was assumed with an uplift of 0.04 mm/yr based on Evenstar et al. (2015b).

To enable comparison of the new with previous results (Dunai et al. 2004, Evenstar et al. 2009), previous ages were recalculated using the same method detailed above (Data repository B).

4. Results

4.1 Stratigraphy

The regional chronostratigraphy is summarized in a north-south transect running from 16°S to 22°S (Figure 8) and in a paleogeographic map of the main stratigraphic

stages (Figure 9). Six age-based and regionally extensive stratigraphic units (Units 1-6, Figure 8) are recognised : Late Oligocene (~35-23 Ma); Early Miocene (23-19 Ma); Early to Mid Miocene (~18-13 Ma); Mid Miocene (~12-11 Ma); Late Miocene to Early Pliocene (~8-7 Ma); and Late Pliocene (~5-3 Ma). Deposition of each of these units ceased abruptly, marked by hiatuses dated at ~23 Ma, ~19 Ma, ~13 Ma, ~11 Ma, ~7 Ma and ~3 Ma. These units differ somewhat from those defined by Jordan et al. (2010). The lowest unit dated at 30 to 20 Ma by Jordan et al. (2010) is here separated into two units, Unit 1 (~35-23 Ma) and Unit 2 (~23-19 Ma). Units 3 and 4 correspond respectively to the second unit (~20 Ma -16 Ma) and the third unit (~14-10 Ma) of Jordan et al. (2010). The youngest unit of Jordan et al. (2010) at ~7-3.5 Ma is here separated into two units; Unit 5 (8 Ma to ~7 Ma) and Unit 6 (5 to 3 Ma).

Unit 1 (35 to 23 Ma) is dominated by conglomerates and is termed the Azapa Formation and is also known by other names: Lower Moquegue Formation; Lower part of the Altos de Pica Formation; Tambores Formation; and the Calama Formation (Figure 8; Hartley and Evenstar 2009; Wotzlaw et al. 2011; van Zalinge et al. 2016a). These deposits represent shedding of sediments off the emerging Andes (Garcia and Hérial 2005) and have been dated using interbedded volcanic deposits (summarised in Hartley and Evenstar 2009). The sediments infilled the Longitudinal Valley and partially infilled the basins in the Coastal Cordillera, forming a regional aggradational surface that originally graded down to the coast (Noble et al. 1985 and Dunai et al. 2005). Around 23 Ma, sedimentation ceased in the Coastal Cordillera, parts of the Longitudinal Valley, and the Calama Basin (Dunai et al. 2005, May et al. 2005; Quang et al. 2005, Jordan et al. 2015, Alván et al. 2015). This hiatus in sedimentation is represented by the Tarapaca Paleosurface in the Coastal Cordillera of northern Chile (Mortimer and Saric 1972 and Figure 1B), dated at ~23 Ma with CN surface exposure dating (Dunai et al. 2005), and the Altos de Camilaca palaeosurface in the Longitudinal Valley and Precordillera of southern Peru, dated at ~24 Ma using volcanic ashes that underlie and overlie the surface (Quang et al. 2005). The Coastal Cordillera started to uplift shortly after this period becoming a substantial barrier to westward flowing sedimentary systems (Delouis et al. 1998, Hartley et al. 2000, Wörner et al. 2002, Dunai et al. 2005, Armijo et al. 2015, Madella et al. 2016) except

around the Bolivian Orocline were uplift rates were much lower (Madella et al. 2016). Uplift rates are poorly constrained but generally believed to have been between 0.04 mm/yr to 0.07 mm/yr (Delouis et al. 1998, Dunai et al. 2005).

Unit 2 (23-19 Ma) consists of a series of sediments and volcanic deposits that were emplaced after 23 Ma. In the southern Longitudinal Valley, this unit forms part of the Altos de Pica Formation conglomerates and towards the Bolivian Orocline, (Figure 8) becomes increasingly dominated by ignimbrites of the Oxaya Formation (dated at 23-19 Ma; van Zalinge et al. 2016a). To the north of the Bolivian Orocline, the volcanic deposits are increasingly interbedded with terrestrial sediments and form the Huaylillas Formation (or Moquegua "C" of Quang et al. 2005, Thouret et al. 2011). Within the Coastal Cordillera in southern Peru, a series of propagating clinothems of the Camaná Formation were deposited (Alván et al. 2015). At 19 Ma, deposition ceased throughout the region. This hiatus is represented by a previously unrecognised paleosurface in northern Chile and the Pampas Lagunas paleosurface in southern Peru (dated using volcanic deposits that underlie and overly the surface (Quang et al. 2005; Figure 1B).

Unit 3 (~19-13 Ma) was recognised throughout the region except for around the Bolivian Orocline (18°30'S and 18°00'S; Figure 9C). In southern Peru, this unit consists of dated ignimbrites, fluvially reworked volcanic sediments and lahar deposits of the Chuntacala Formation (Thouret et al. 2007, Decou et al. 2011), as well as clinothems of the Camaná Formation (Alván et al. 2015). Within the Longitudinal Valley of northern Chile, Unit 3 consists of a series of fluvial gravels termed the El Diablo Formation or upper Altos de Pica Formation (Figure 8). Towards the south, between 19°30'S and 20°30'S, Unit 3 includes the Tambillo ignimbrite (Galli, 1968) and the Huasco ignimbrite (~16 Ma; Galli, 1968; Vergara and Thomas 1984). Alluvial fans of Unit 3 (the Lasana Formation) flank the Calama Basin margin with thick mudstone deposited within the center (Jalquinche Formation) (May et al. 2005; Jordan et al. 2015 and Figure 9C). Age constraints on this unit are based on interbedded volcanic deposits throughout the region, most notably the Nama ignimbrite (or Altos de Pica Formation member 4) dated at ~16.27 ± 0.16 Ma, which

can be found from 19°S to 20°30'S (Victor et al. 2004). A large, ~13 Ma regional unconformity is recognized throughout northern Chile and southern Peru with cessation of sedimentation everywhere except within the Calama Basin. However, on the edge of the Calama Basin a prominent palaeosol (Barro Arana Geosol) formed along the south-eastern flank of the Calama Basin is dated at 13-8 Ma (Hartley & May 1998; Rech et al. 2006).

Unit 4 (12-11 Ma) consists of a series of thick gravels and corresponds to upper parts of the El Diablo Formation in the Longitudinal Valley and the Lower Vilama Formation in the Pre-Andean Basin (Evenstar et al. 2015a). Age constraints in the Longitudinal Valley on Unit 4 are based on volcanic deposits interbedded with the sediments at 19°30'S dated at 11.7 ±0.4 Ma (Farías et al. 2004) and the Tana Lava dated at 8.2 ± 0.5 Ma (Munoz and Sepulveda 1992) that overlies the paleosurface at 19°20'S, constraining the age of the surface as 11.7-8.7 Ma (Hoke et al. 2007). In southern Peru, Unit 4 correlates with the sandstone-rich Maure Formation in the Longitudinal Valley and fluvial gravels of the Camaná Formation in the Coastal Cordillera (Alván et al. 2015). At ~11 Ma regional sedimentation ceased and is represented by a hiatus, which is recognized in southern Peru as the Pampa Sitana paleosurface dated using volcanic deposits that underlie and overlie the surface (Quang et al. 2005).

Unit 5 (8-7 Ma) consists of a series of sandstones and mudstones termed the Hilaricos Formation and corresponds to the deposition of several thick alluvial fans in the Chilean Longitudinal Valley dated using underlying and overlying volcanic deposits (Kiefer et al. 1997, Sáez et al. 2012). Within the Pre-Andean basins, coarse conglomerates of the Vilama Formation and Chiquinaputo Formation were deposited within the Salar de Atacama and Calama Basin respectively (Evenstar et al. 2015a; May et al. 1999; 2005). In southern Peru, fluvial sandstones of the Maure Formation were deposited in the Longitudinal Valley and a series of fluvial conglomerates (Camaná Formations) prograded into the Pacific Ocean from the Coastal Cordillera (Alván et al. 2015). At ~7 Ma sedimentation ceased (Figure 8). In southern Peru, the top of this unit is represented by the Cerro Sagollo paleosurface

(>7.9 Ma based on dated volcanic ashes) (Quang et al. 2005). In the Chilean Longitudinal Valley, the alluvial red beds were deposited between 7.8 ± 0.2 Ma and 6.8 ± 0.2 Ma at the Arcas fan (21°40'S) and within the Quillagua-Llamara Basin ceasing by 5.3 Ma (based on dated ashes that underlie and overlie the surface; Kött et al., 1995; Sáez et al. 2012). To the south in the Pre-Andean Basins, the Calama and Quillagua-Llamara Basins merged (May et al. 2005).

Unit 6 (~5-3 Ma) consists of a series of diatomite and mudstone beds in the Longitudinal Valley south of 21°S, termed the Quillagua Formation, and a series of carbonate and mudstone beds in the Pre-Andean Basins, termed the Opache and Vilama Formation based on dated volcanic deposits in the region (Jordan et al. 2010; 2015, Evenstar et al., 2015a). In southern Peru, this correlates with the upper parts of the Moquegua "D" Formation conglomerates. Large-scale sedimentation throughout the region ceased at ca. 3.6-3 Ma, with widespread evaporates developed after this time (based on volcanic deposits interbedded within the evaporates and paleomagnetic studies within the region; Hartley et al. 2000; Sáez et al. 2012; Jordan et al. 2014). Post-3 Ma sedimentation within the region is restricted to small-scale pluvial events that only deposit a thin veneer of sediments in the region (Nester et al. 2007, Jordan et al. 2014).

The regional extent of these units varies in space and time (Figures 8 and 9). Units 1 and 2 extend across the whole region. They reach a combined thickness up to 1000 m at the Bolivian Orocline and thin to ~400 m towards the south (Sections S, T and U in Figure 3). Units 3 and 4 are absent from cross-section S and thicken towards the south from ~100 m each at cross section T to ~250 m each at cross-section U. Stratigraphic Units 5 and 6 are only present in the southernmost cross-section U with a thickness of up to 250 m.

There is variation in the distribution of the stratigraphic units from east to west (Figure 3). In cross-section S (Figure 3), the oldest Unit 1 thickens markedly to the west of the Ausipar Fault. Substantial erosion has occurred over the Huaylillas Anticline (van Zalinge et al. 2016b), indicating that Unit 2 originally thickened

towards the east. The current paleosurface of this region is formed on Unit 2. Within cross section T (Figure 3), Unit 1 is thickest within the centre of the basin. Unit 2 is thickest on the eastern edge of the basin and is exposed at the surface in the west Both Units 3 and 4 are found as a thin veneer throughout the central part of the basin. In cross section U (Figure 3), the sediments were deposited within two basins separated by the Altos de Pica (AdP) Basement High. The eastern basin contains the thickest deposits of Units 1 and 2 within the centre of the basin, with Unit 3 showing the greatest thickness on the eastern edge of the basin. Units 4, 5 and 6 are deposited as a lens shaped feature within both of the basins, with Units 5 and 6 thickest in the eastern basin.

4.2 Large-scale mapping of the Pacific Paleosurface

Satellite imagery was used to characterise the different surfaces that make up the PPS (Figure 10). Surfaces can be defined using five criteria: (1) colour in VNIR (Visible Near-Infrared) and SWIR (Shortwave Infrared); (2) difference in surface texture; (3) surface roughness; (4) angle of slope; and (5) direction of slope (aspect).

These criteria reflect the variations in character of the regional surfaces (described in section 3.2) as well as recording larger scale features (described below). Surface texture was characterised using different drainage patterns defined using the criteria of Ritter (2006) and tectonic features such as preservation of fault scarps on the surface. The slope map (Data repository A) records the depositional angle of the surfaces and also later tilting events. The depositional angle of the surface can depend on several factors including water discharge, sediment supply, grain size and transport mechanisms. However, modern distributive fluvial systems (Weissman et al. 2010) in northern Chile have depositional surfaces with an angle in the range of 1° to 3°. Older paleosurfaces within the Longitudinal Valley have a greater slope with angles up to 10-20° proximal to the Altos de Pica Basement high, suggesting substantial post depositional tilting (Jordan et al. 2010), an interpretation supported by field observations (Figure 11C). The slope direction can help identify the distinct

apex point of a distributive fluvial system and highlight any significant changes in incision or deposition of the distributive fluvial systems through time.

The PPS can be divided into eight distinct geomorphic surfaces, five aggradational surfaces (AS1-5) and three degradational surfaces (IDN1 and DS2-3), which can be correlated with the stratigraphic hiatuses (Figure 8). The aggradational surfaces mark the top of sedimentary successions that form the stratigraphic units, whilst degradational surfaces cut into and truncate the underlying sediments or rock packages. Hiatuses are also recorded as unconformities in the subsurface or as an abandoned aggradational surface. Below we describe the characteristics and regional distribution of each surface, which are presented in Table 2, Figure 6 and Figure 10.

4.2.1 Aggradational Surfaces

Aggradational Surface 1 (AS1) forms the recent (Quaternary) depositional surface, which is white in the visible spectrum, pale blue in Landsat images, and crosscuts all older surfaces. Fluvial surface morphologies are easily recognised on satellite images (Figure 10). The white colour is caused by the high mud and sand content in the matrix of deposits and absence of desert varnish on clasts (Figure 4B and 11A). The surfaces are characterised by low slope angles of approximately 0-5° (Figure 11C) and have no preferred slope direction (Figure 10). On the DEM map the surface appears smooth at the 30 m scale, but in the field is characterised by 10-100 cm scale topography with well-defined depositional features, such as bar and swale and occasional vegetation (Figures 4B, 10 and 11B).

AS1 is characterised by a series of distributive fluvial systems from 19°50'S to 21°S (Figure 6). The apex point of these fans is located within the centre of the Longitudinal Valley, ~ 30 km west of the Precordillera and ~25 km east of the Coastal Cordillera. The Altos de Pica basement high controls the location of the apex of the fans. South of 21°S, the width of the Longitudinal Valley decreases from 60 km to 30 km (Figure 6). The fan apices migrate to the east here and are located on the edge of

the Precordillera. AS1 distributive fluvial systems terminate in playa lake deposits along the western edge of the Longitudinal Valley south of 19°30'S and increase in E-W width from 10 km to 30 km towards the south. AS1 deposits are predominately formed from mudflows and relates to the small-scale sedimentation within the Quaternary. This surface does not define a stratigraphic unit, being a minor sedimentary veneer in the basin.

Aggradational Surface 2 (AS2) is grey to pink brown in the visible spectrum and grey to pink brown on false colour images due to the increased prominence of desert varnish on the clasts (Figure 10). The surface slopes at an angle between 0-5° and has a dominant slope direction to the west. Depositional features such as bar and swale can still be easily recognised both in the field and on satellite images (Figure 10). AS2 is only found south of 20°45'S (Figure 6). The surface also occurs north of this region (20°45'S), but here the deposits contain predominantly ignimbrite clasts, making this surface hard to distinguish on satellite images from older surfaces developed on ignimbrite. From 19°50'S to 21°S, a series of distributive fluvial systems (~30 km in length) are preserved on the eastern side of the AdP basement high. To the west of the AdP basement high, AS2 could be present but are covered by deposits of younger AS1. To the south of 21°S, where the Longitudinal Valley decreases in width fan apices migrate to the east and are located on the edge of the Precordillera. AS2 correlates with the Stage NII paleosurface of Jordan et al. (2014) dated between 4.3 – 2.5 Ma. Its regional extent and preservation is consistent with AS2 marking the end of deposition for stratigraphic unit 6 (Quillagua Formation).

Aggradational Surface 3 (AS3) is only found south of 19°45'S, where it consists of several large alluvial fans that are pale brown to dark red in the visible spectrum and dark, blue-grey to dark red in false colour (Table 2 and Figure 10). The dark colour is due to well-developed desert varnish on the clasts and development of interlocking clasts of the desert pavement masking the underlying sand and mud matrix. The fans can be easily identified on maps by their radial slope direction (Figure 10) and the higher slope angle relative to younger surfaces of 2.5-7.5° (Figure 10). Fluvial channel features can be recognised on satellite images and in the field, but are less clear than

on AS1 and AS2 (Figure 10). Between 19°45'S and 21°S these fans are up to 30 km in length with the apex of the fan along the edge of the AdP basement high in the centre of the Longitudinal Valley (Figure 6). To the south of 21°S, the fans extend across the Longitudinal Valley with the apex point of the fans within the Precordillera. AS3 correlates through to the surface of the Arcas fan (21°40'S), which has been constrained as forming between 7.8 ± 0.2 Ma and 6.8 ± 0.2 Ma (Kiefer et al. 1997) and marks the end of stratigraphic unit 5.

Aggradational Surface 4 (AS4) is found from 18°S to 21°S (Figure 6). In the north the surface varies from dark brown to orange in the visible spectrum and dark brown to green in false colour images (Table 2 and Figure 10). In the south, the surface changes in character to red brown in the visible spectrum and dark red brown in false colour. These colour changes are attributed to the increasing importance of ignimbrite in the source region to the south and a well-developed desert pavement with thick desert varnish on clasts. AS4 shows no clear fan shapes on the slope direction map. Surface slopes are typically 5-7.5° with a south west-facing dominant slope direction inferred to result from post-depositional tilting. The surface itself shows no clear depositional structure. However, throughout the region AS4 is covered by a series of fluvial channels seen as greyish blue in the visible spectrum to blue grey in false colours (Figure 10). These channels predominantly incise into or deposit onto AS4 to the east and west of the Longitudinal Valley, respectively. The channels suggest significant modification of AS4 by younger events although in the field they are commonly shallow superficial features (Figure 11D). These later events most likely correlate with AS2 and AS3.

AS4 is only present in the centre of the Longitudinal Valley and is absent around the Bolivian Orocline (18°10'S and 18°20'S). From 18°20'S to 19°20'S the surface is deeply incised (up to 1000 m) by the main east-west quebradas and by several degradational surfaces along the eastern side of the Longitudinal Valley (described below). As such the surface is only preserved in isolated patches (Figure 6). Between 19°20 and 21°S, the surface forms a composite feature with multiple later fluvial channels superimposed on top of the surface. Between 20°10'S and 20°40'S there is

increased ignimbrite within the source region, making recognition of modification events difficult to recognise. South of 21°S, AS3 is covered by deposits related to AS1, AS2 and AS3. The regional distribution and preservation of the surface suggests it represents the end of deposition of the El Diablo Formation.

Aggradational Surface 5 (AS5) is the oldest surface recognised in the Longitudinal Valley. Within the hillshade map this surface shows an undulating topography and in the field is underlain by thick (3-4 m) gypcrete soils (Figure 4E), which inflate at differing rates creating a puffy appearance at ground level (Figure 4F). The surface lacks depositional features due to either a well-developed desert pavement or absence of desert pavement revealing the underlying soil (Figure 10). The only features recognised on the surface are fault scarps (Figure 4A).

North of 19°45'S, the surface is identified by its white colour in both the visible spectrum and false colour images (Figure 10). This colour is attributed to gypcrete soil exposed at the surface due to absence of desert pavement clasts. The matrix of the surface constitutes approximately 65% sand and 20% gypcrete (Figure 4G). To the south of 19°45'S, the surface changes to a uniform dark colour. In this region, the desert pavement is characterised by an even distribution of clasts with thick red to brown desert varnish and a matrix consisting of 80% sand to pebble-sized clasts (Figure 4C).

The slope and slope direction of AS5 varies across the region. Between 18°40'S and 19°S the surface shows an average range of direction from 0-7.5° to the north, whereas between 19°30'S and 19°'S the surface shows an average range of slope direction from 0-7.5° to a south. This change in slope is associated with a large-scale fold with an axis running east-west at 19°'S. South of 19°45'S, the surface slopes at westward angle of 5-15°, indicative of post depositional tilting. This interpretation is supported by studies in the south Longitudinal Valley (Jordan et al. 2010) and by field observation in the Cerro Colorado region that show the older surface at a higher angle and incised by a lower angle younger paleosurface (Figure 11C).

AS5 is preserved on the western edge of the Longitudinal Valley proximal to the Coastal Cordillera between 18°30'S and 19°45'S (Figure 6). The surface varies in width between 15-20 km and is adjacent to AS4 to the east. Within this region the ignimbrites of the Oxaya Formation directly underlie part of the surface south of 19°S constraining the surface to representing the end of stratigraphic unit 2. To the south of 19°45'S, the surface is overlain by the younger aggradational surfaces (AS1 and AS3) and is only preserved as isolated patches within the central part of the Longitudinal Valley until 20°25'S. To the south of 20°25'S the surface is completely buried by younger aggradational surfaces.

4.2.2 Degradational surfaces.

A series of degradational surfaces and an incised degradational network are identified across the Longitudinal Valley. The basin can be divided on the basis of drainage type (external or internal) into two areas. North of 19°30'S exorheic (external) drainage predominates and the terminal base level is sea level, at the Pacific Ocean. South of 19°30'S, drainage is endorheic (internal) and the terminal base level is located within the Longitudinal Valley at the much higher elevation of 1000 m.

Exorheic Degradational Surfaces

Within the northern area, 3 distinct drainage networks can be identified and mapped (Figure 6). The older two drainage systems (DS2-3) form two regionally extensive degradational surfaces whereas the youngest drainage network (Incised Drainage Network-IDN1) deeply incise all these surfaces, forming the modern day rivers. The degradational surfaces (DS2-3) show increasing incision into the underlying stratigraphy within the Longitudinal Valley (Figure 6B). The drainage networks converge at points controlled by underlying tectonic structures (Garcia and Hérial 2005).

The youngest incised drainage network (Incised Degradational Network 1 - IDN1) is the modern trellis degradational network formed by the five main rivers, Quebradas Lluta, Azapa, Victor, Camarones and Tana. The rivers incise up to 1700 m into the PPS (Figure 6).

The second youngest drainage network (Degradational Surface 2; DS2) is recognised from 17°50'S to 19°S. The surface runs along the eastern edge of the Longitudinal Valley, shows a parallel drainage pattern and slopes of 0 to 5° (Figure 10). The surface is orange to cream brown in the visible spectrum and orange to pale pink in false colour image (Figure 10). The surface slopes to the west except for a small region between 18° 20'S and 18° 10'S where the eastern edge of the surface is tilted towards the east due to folding (van Zalinge et al. 2016b). The surface incises into DS3 and completely erodes the El Diablo Formation and the youngest member of the Oxaya Formation in this area, the Oxaya Ignimbrite, (Figure 6; van Zalinge et al. 2016a). The degradational surface forms on top of the Cardones ignimbrite (the lowest ignimbrite member of the Oxaya Formation; van Zalinge et al. 2016a).

Degradational Surface 3 (DS3) is recognised from 17°40'S to 19°S (Figure 6) and shows a dendritic drainage pattern. The surface is pink to orange cream in the visible spectrum and pale blue to white orange in false colour (Figure 10). The surface slopes at between 2.5 to 7.5° to the west suggesting post-incision tilting. Between 17°40'S and 18° 10'S and between 18° 20'S and 19°S the surface is preserved within the centre of the Longitudinal Valley between AS4 to the west and DS2 to the east. Between 18°10'S and 18° 20'S, the surface extends to the Coastal Cordillera. To the south of 18°50'S, within the catchment of Quebrada Camarones, this surface forms a terrace within the main quebrada. DS3 incises (Figure 6B) up to 90 m into AS4, removing the El Diablo Formation. The degradational surface forms on top of the underlying Oxaya Ignimbrite.

Endorheic Degradational Surfaces

South of 19°30'S the Longitudinal Valley is endorheically drained and hosts 2 sets of degradational surfaces which correlate through the exorheic region in the north (Figure 6). The youngest IDN1 is only recorded on the eastern side of the Longitudinal Valley from 19°30'S to 21°S. Throughout this region the inception point between aggradational and degradational systems forms within the centre of the Longitudinal Valley overlying the AdP basement high. South of 21°S the Longitudinal Valley decreases in width and the incisional drainage is confined to the Precordillera.

South of 20°45'S, a drainage network associated with DS3 can be recognised and correlated through to AS3. The surface shows a dendritic drainage network with a high angle of 2.5° to 7.5° sloping to the West. The surface colour varies from pink to yellow grey in normal light and dark blue grey to dark olive green in false colour. The surface decreases in width across the Longitudinal Valley from 25 km in the north to 5 km south of 21°30'S.

4.2.3 Large-scale surface variations

The Chilean Longitudinal Valley can be divided into 3 geographic zones (here referred to as regions 1 to 3) based on surface mapping (Figure 6).

Region 1 (18°S to 19°20'S) consists of remnants of AS5 on the western edge of the Longitudinal Valley and south of 18°30'S and AS4 in the centre of the valley. To the east of these aggradational surfaces, two degradational surfaces (DS2 and DS3) increasingly incise aggradational surface 4 and the underlying Oxaya Formation. Drainage networks associated with the degradational surfaces have completely eroded large parts of the PPS on the western edge of the Longitudinal Valley and show an increase in incision into the PPS towards the Bolivian Orocline. The modern quebradas (IDN1) deeply incise all these surfaces, with the four main rivers cutting east to west and draining into the Pacific Ocean.

Region 2 (19°20'S to 21°S) includes Quebrada Tana, which terminates in the Pacific Ocean, and some smaller rivers to the south, which terminate within the

Longitudinal Valley. The region is dominated by AS4 within the central and eastern part of the Longitudinal Valley with later modification of this surface by shallow degradational and aggradational events. South of 20°S, AS3 is partially overlain by younger distributive fluvial systems (AS1-3). Along the western edge of the Longitudinal Valley the surfaces vary. North of 19°50, AS5 is preserved whereas south of this AS1 sediments predominate. The surfaces changes in depositional style from aggradational to degradational related to the underlying AdP basement high. This basement high (cross section U in Figure 3) separates the Longitudinal Valley into two basins.

Region 3 (21°S to 22°20'S) contains predominantly recent distributive fluvial systems (AS1-3) including the Arcas fan. Within this region the western basin present in Region 2 pinches out and the Longitudinal Valley is formed from only the thinner eastern basin. In this region the distributive fluvial systems originate from the Precordillera and cover older depositional surfaces (AS5 and AS4). North of 21°30S these distributive fluvial systems drain into large salt flats, whereas to the south the surfaces are drained by the Rio Loa.

4.3 Elevation Profiles

4.3.1 Longitudinal elevation profiles

The North-South elevation profiles show marked variations (Figure 7). Profile A, along the eastern edge of the Longitudinal Valley, varies in elevation from 800 m at 17°40'S to 2400 m at 20°S. The profile shows a plateau of high elevation between 19°S and 21°S, with an average height of ~2200 m. The lowest elevation occurs around the Bolivian Orocline with the elevation reducing to ~1200 m at 18°20'S. The preservation of the PPS across this area varies dramatically. From 19°20'S to 18°S, the paleosurface is absent due to lack of deposition or erosion with an average of 250 m height difference between the projected PPS and the current elevation. South of this area down to 21°S, the paleosurface is preserved as isolated remnants

separated by drainage systems that incise several tens of m and locally up to 300 m into the surface. South of 21°S, the paleosurface is completely preserved.

Profile B is proximal to the Coastal Cordillera. Similar to profile A it shows the lowest elevation at the Bolivian Orocline, of 50 m at 18°20'S, with increasing elevation to the north and south. However, in contrast, profile B displays a peak in elevation of ~1100 m at 19°20'S which slowly decreases to the south reaching an elevation of 750 m at 21°S. The PPS is generally well preserved along this profile, except north of 19°30'S where the surface is incised up to 750 m by the four northernmost rivers.

The elevation difference between the eastern and western edge of the Longitudinal Valley varies across the area, partly reflecting changes in the Valley width. Between 18°S to 19°20'S, the basin is exorheic, the Valley is 60-70 km wide and shows the highest difference between the two profiles of 1400-1100 m. From 19°20'S to 21°S, the basin switches to endorheic drainage with the difference in elevation profiles being approximately constant at 1100 m. From 19°50'S to 21°15'S the area is underlain by two basins separated by the N-S striking AdP basement high (Figure 6). To the south of 21°15'S, in Region 3, the western basin pinches out and the Longitudinal Valley decreases to half the width ~30 km and the difference in elevation between the two profiles decreases (700 m to ~500 m) as the two profiles become closer.

4.3.2 Longitudinal river profiles

Longitudinal profiles of six rivers show distinct differences running from north to south (Figure 2). The four northern most rivers (1-4: Lluta, Camarones, Victor and Tana) drain into the Pacific Ocean whereas the two southern rivers (5-6: Aroma and Tiquima) drain into the Longitudinal Valley. Within the three southernmost rivers (rivers 4, 5 and 6) the elevation difference between the paleosurface and modern river profile decreases towards the west until they merge within the centre of the Longitudinal Valley. The two southernmost rivers (Aroma and Tiquima) show no elevation difference west of this point. River profile 4 (Tana), however, shows a

knickpoint within the Coastal Cordillera with the profiles increasing in elevation difference towards the Pacific Ocean. The three northernmost rivers (Lluta, Camarones and Victor) show complete vertical separation between the paleosurface and modern rivers of at least 500 m. River profile 3 (Camarones) shows a knickpoint within the eastern Longitudinal Valley whereas the two northernmost rivers (Lluta and Victor) both show knickpoints within the Precordillera (Garcia et al. 2011). The two northernmost rivers (Lluta and Victor) show large elevation differences in the eastern Longitudinal Valley associated with folding of the PPS to form the Oxaya and Huaylillas Anticlines.

Four river valley cross-sections were constructed across the four northernmost rivers (1-Lluta, 2- Victor, 3- Camarones and 4- Tana; Fig. 2c) proximal to the Coastal Cordillera (Figure 2). Section 4 (Tana) shows minor incision of ~100 m with a valley width of 0.5 km. Section 3 (Camarones) shows a classic V-shape valley with incision of 600 m and valley width of 2.5 km. Section 2 (Victor) shows a wider V-shape valley with incision of 600 m and valley width of 3.5 km. Section 1 (Lluta) shows a wide valley with incision of 200 m and valley width of 4 km.

4.4 Cosmogenic ^{3}He and ^{21}Ne data

Cosmogenic ^{3}He and ^{21}Ne data (Figure 5) are used to calculate the minimum deposition age of each paleosurface (Table 1) as erosion and exhumation can lower boulder exposure ages in such long-lived surfaces. The ages are plotted together with previously published cosmogenic surface exposure ages, stratigraphic data and other geochronological information from each surface in Figure 12 and 13. The ages constrain the time when the last large-scale fluvial event occurred on the paleosurfaces. It is likely that the sediments and soil surrounding the boulders on the surface have undergone minor modifications by occasional moisture, soil and aeolian processes since depostion of the boulders as both desert pavements and soil profiles can form a substaintial time after the last major fluvial event (Ewring et al. 2006; Seong et al. 2017).

The oldest cosmogenic exposure age for each surface either overlaps, or is slightly younger than, the surface age based on independent geochronological constraints (Figure 12). All cosmogenic exposure ages from the youngest surface S1 (AS1 and IDN1), equivalent to NV paleosurface of Jordan et al. (2014) and Pleistocene fans documented by Nester et al. (2007), are less than 1.1 Ma. AS2 correlates with the stage NII paleosurface in the southern Longitudinal Valley that is between 4.3 Ma and 2.5 Ma based on two interbedded tephra layers in alluvial sediments (Jordan et al. 2014). The exposure ages cluster between 3.2 and 2.1 Ma, most overlapping with the younger tephra age. The oldest exposure age on AS3 is 7.04 ± 0.32 Ma at sample site 3. AS3 correlates through to the Arcas fan (21°40'S), which is independently dated using underlying and overlying volcanic deposits at between 7.8 ± 0.2 Ma and 6.8 ± 0.2 Ma. Again the oldest ages overlaps with the younger of the two bracketing ages. Surface 4 is an aggradational surface formed by compilation of stratigraphic units 3 and 4. The formation age is bracketed by the underlying Nama ignimbrite (16.27 ± 0.16 Ma) and the overlying Tana lava (8.2 ± 0.5 Ma; Munoz and Sepulveda 1992). This surface formed diachronously from west to east (Figure 3) with the youngest sediments deposited in the centre of the basin. The oldest exposure age on AS4 is ~16 Ma (Evenstar et al. 2009) reflecting the deposition of stratigraphic unit 3, whereas the younger cluster of ages at ~11.3 Ma are consistent with deposition at the end of stratigraphic unit 4. Surface 5 developed in places on the Oxaya Ignimbrite, giving an upper limit of 19.711 ± 0.036 Ma (van Zalinge et al. 2016a). The oldest cosmogenic surface exposure ages (20.17 ± 0.65 Ma at sample site 8 and 18.41 ± 0.25 Ma at sample site 5) are consistent with formation of the surface soon after ignimbrite emplacement. The Tarapaca paleosurface within the Coastal Cordillera contains the oldest exposure ages (23 to 25 Ma; Dunai et al., 2005; Kober et al. 2007), consistent with ages of 22-25 Ma for underlying sediments (Wörner et al. 2002; Dunai et al. 2005). Sample site 14 forms part of the debris deposits from the Lluta collapse which host an exposure age of 2.6 ± 0.06 Ma, in agreement with previous age constraints (Wörner et al. 2002: Kober et al. 2007).

The oldest ages from each surface are consistent with the prevailing stratigraphic constraints and yield ages that are close to independently determined ages. Inheritance of cosmogenic nuclides has been recorded in underlying sediments and clasts (<5 cm) within the small fluvial systems to the south (Gonzalez et al. 2006 and Jungers et al. 2013). However, boulders from this region have been shown in numerous studies to be the most stable part of the landscape and do not record cosmogenic nuclides generated prior to deposition (Dunai et al. 2005, Gonzalez et al. 2006, Kober et al. 2007, Evenstar et al. 2009, 2016, Placzek et la. 2010, Jungers et al. 2013 and Matmon et al. 2015). This study provides no compelling evidence to support inheritance of significant amounts of cosmogenic ^{3}He and ^{21}Ne in these pebbles and boulders. Thus cosmogenic ^{3}He and ^{21}Ne allow the age of Cenozoic surfaces to be determined where chrono-stratigraphic constraints are not available (Figure 13).

Many sites, however, yield boulders/pebbles with exposure ages that are much younger than initial deposition. This complexity may in part reflect post-depositional reworking of surfaces during later wet periods as well as exfoliation of boulder surfaces. Clustering of minimum exposure ages provides evidence for these processes (e.g. Evenstar et al. 2009). Erosion, weathering and burial of the boulders within sediment since deposition also all tend to inhibit cosmogenic nuclide production and effectively lower the age of boulders.

5. Discussion

5.1 Evolution of the PPS

This paper presents the first regional characterisation of the PPS. It combines several different stratigraphic and paleosurface studies with new field observations to identify six distinct stratigraphic units within the Longitudinal Valley. These units can be correlated over a distance of 800 km (16°S to 23°S) and represent discrete periods of increased sediment supply separated by hiatuses (denoted by

unconformities and disconformities) where sediment supply was substantially decreased.

The PPS has been mapped using multispectral satellite data and a digital elevation model between 18°S and 22°S. Eight distinct paleosurfaces (5 aggradational surfaces and 3 degradational networks which encompass 1 incisional network and 2 degradational surfaces) have been identified with different morphological and textural features. These surfaces can be traced regionally, with erosion and deposition occurring contemporaneously on the same time horizon in different locations (Figure 14). Forty five new cosmogenic ^{3}He and ^{21}Ne surface exposure ages are combined with previously published ages, stratigraphic data and other geochronological information to constrain the timing of surface formation to ~23 Ma, ~19 Ma, ~11 Ma, ~7 Ma and ~3 Ma. Formation of the surfaces, by the cessation of depositional or large-scale erosional processes, is found to coincide closely with the timing of the hiatuses (at the top of sedimentary and volcanic units) as shown below.

Stratigraphic Unit 1 is recognised throughout the Longitudinal Valley and occurs in the Coastal Cordillera. Uplift of the Cordillera post 23 Ma isolates the basins within the Coastal Cordillera from later sedimentation forming the regionally extensive Chilean Tarapaca paleosurface and Peruvian Altos de Camalaca paleosurface (Figure 1B). The age of this hiatus is at ~23 Ma. Minor reworking events post-23 Ma are recognised at ~20 Ma, 14 Ma and 10 Ma (Dunai et al. 2005).

Within the Longitudinal Valley stratigraphic Unit 2 directly overlies Unit 1 with no pause in sediment deposition. The top of Unit 2 can be recognised along the western edge of the Longitudinal Valley (Figure 3 and Figure 4H) as an aggradational surface (AS5). Within the Longitudinal Valley, maximum exposure ages for Surface 5 vary from 20.17 ± 0.65 Ma to 18.41 ± 0.25 Ma.

Stratigraphic Units 3 and 4 are present throughout the Longitudinal Valley except between 18°10'S and 18°30'S. Although these units ceased at differing times, the

surface has the same characteristics from multispectral satellite mapping. Therefore, we suggest that they form the same surface, AS4, which formed diachronously with the oldest ages from this surface at ~16 Ma representing the end of stratigraphic unit 3 and the main depositional phase at the end of stratigraphic unit 4 at ~11 Ma (Quang et al. 2005; Evenstar et al. 2009). This surface was then substantially reworked when Surfaces 2 and 3 were created.

Stratigraphic Unit 5 is associated with both AS3 and DS3. From 18°S to 19°S, the timing of deposition of stratigraphic Unit 5 coincides with the formation of degradational surface (DS3), which cuts into and erodes AS4. The age of DS3 is constrained to <8 Ma by cosmogenic exposure ages on the surface at 18°42'S (a single age of ~5.3 Ma; Kober et al. 2007), on a lower terrace within Quebrada Camarones (7.15 ± 0.14 Ma and 6.49 ± 0.12 Ma; sample site 15, *this study*) and as reworking of AS3 at 18° 50'S (5.26 ± 0.12 Ma and 7.9 ± 0.15 Ma; sample site 16, *this study*). From 19°00'S to 20°15'S this event is only recognised as reworking of the older AS4 dated using 10 cosmogenic exposure ages (sample sites 3, 4, 6 and 7, *this study)* and 5 samples from Quebrada Aroma (Evenstar et al. 2009). South of 20°15'S, stratigraphic Unit 5 constitutes a series of distributive fluvial systems which, when abandoned, formed an aggradational surface (AS5) with a surface exposure age of ~5.3 Ma. This date is derived from cosmogenic isotope dating in this study, interbedded volcanics within the fluvial sediments (Kiefer et al. 1997) and paleosols (Jordan et al. 2014).

Surface 2 (both AS2 and DS2) represents the end of deposition of stratigraphic Unit 6. From 18°00' S to 18°50'S this surface forms a degradational surface (DS2) that cuts into and erodes DS3. Within the Longitudinal Valley from 18°14'S to 18°42'S, the age of incision is constrained by a cosmogenic surface exposure age of ~3.5 Ma to ~2 Ma on DS2 in the east (7 samples; Kober et al. 2007). Between 19°00'S to 19°45'S this surface is only represented through the time AS4 was reworked at ~ 3.5- 2 Ma (sample site 20; *this study* and 6 samples from the Quebrada Aroma published in Evenstar et al. 2009). South of 20°45'S, the end of stratigraphic Unit 6 is revealed by numerous relict distributive fluvial systems which are dated at ~3 Ma using paleosols

(Jordan et al. 2014). This time period also corresponds to relict surfaces dated using cosmogenic isotope ages further south in the Pre-Andean basins (Placzek et al. 2010).

In southern Peru, the timing of the four paleosurfaces in the region (Altos de Camilaca at 24-23.8, Pampas Lagunas at 20-19 Ma, Pampa Sitana at 10.1-10 Ma Ma, and Cerro Sagollo at 7.9) correlate with the Tarapaca paleosurface in the Coastal Cordillera and the three oldest paleosurfaces mapped in the study area (Surfaces S3-5). The only surface not correlated through is the Cerro de las Chulpas surface (13-15 Ma), which is recognised as stratigraphic unit 3 but cannot be considered an individual paleosurface in our study area. In northern Chile, between 21°S to 22°S, five stages of paleosurface formation (Stages NI at 11 Ma, NII at 4.5 Ma, NIII at 3.6 Ma, NIV at 2.1 Ma and NV after 1 Ma) are recognised (Jordan et al. 2014). Stages NI, NIII and NV correlate well with the youngest three paleosurfaces recognised in this study (Surface 4, 2 and 1). However, based on the stratigraphic units, mapped paleosurfaces and cosmogenic exposure ages we propose that a separate paleosurface (Surface 3) formed at ~7 Ma which correlates through to the Cerro Sagollo in southern Peru.

It has been suggested that the PPS formed during a narrow time interval between 14 Ma and 10 Ma (e.g. Galli-Oliver 1967, Tosdal et al. 1984, Alpers and Brimhall 1988, Farías et al. 2005, Hoke et al. 2007). However, our regional analysis confirms that the PPS is not a single coherent surface formed in a narrow window of time but a complex surface that has experienced both sedimentation and fluvial erosion since at least the early Miocene, much earlier than previously suggested (e.g. Galli-Oliver 1967, Tosdal et al. 1984, Alpers and Brimhall 1988, Farías et al. 2005, Hoke et al. 2007, Evenstar et al. 2009 and Jordan et al. 2014). Since that time the PPS has developed episodically up until the present day (Jordan et al. 2014) and should instead be termed the Pacific Paleosurfaces.

5.2 Analysis of river profiles

When the terminal base level for a fluvial system shifts the drainage will attempt to adjust to that new base level, although response time may vary spatially depending on sediment supply and fluvial connectivity (Mather et al. 2016 and references therein). If the terminal base level falls rapidly the fluvial system may develop a knickpoint that migrates upstream, lowering the river profile. Consequently rivers first incise vertically and then retreat headward (Schumm et al. 1984). The valley profile typically shifts from minor vertical incision to deep vertical incision with a narrow valley width with limited valley widening (e.g. Bull 1977). The valley slopes will stabilise through slope failure, increasing valley width until stable slope angles are achieved (Mather et al. 2002). How quickly the river and valley adapts to changing base levels depends on factors such as bedrock lithology (erodability) and water and sediment discharge rates, which can vary through time due to river capture events, tectonic uplift or climate change (e.g. Mather et al. 2002, Anton et al. 2015).

Within northern Chile (18°20'S-19°20'S), the four northernmost elevation profiles (1-4 of Figure 2) of the paleosurface proximal to the rivers show that these paleosurfaces initially graded down to a relatively higher elevation base level than today. The present day river profiles currently grade down to the Pacific Ocean. The two northernmost rivers (Lluta and Victor) show significant knick points within the Precordillera and relatively wide, open valleys with landslips, whereas River 3 (Camarones) shows a narrower valley with steeper sides and knick point within the eastern Longitudinal Valley. River 4 (Tana) shows a knickpoint within the Coastal Cordillera and minimal vertical incision in the valley cross-section whilst the two southernmost rivers (Aroma and Tiquima) show no vertical incision to the west. In summary, the river long profiles and sections (Figure 2) suggest that either the rivers incised more rapidly in the north or diachronously across the region.

The variation in timing of incision between the rivers could be due to differences in underlying lithology, stream power or timing of when base levels were modified. Each of which are discussed below.

In Northern Chile the rivers (except Quebrada Lluta) incise through both the Longitudinal Valley and the Coastal Cordillera. The Longitudinal Valley largely hosts weaker sedimentary and volcaniclastic strata whereas the Coastal Cordillera hosts mechanically stronger igneous rocks (Mather and Hartley 2006). However, the width and height of the Coastal Cordillera varies across the region (Figure 7) from 65 km wide and 1000 m high at 22°S, to completely absent at 18°30'S, suggesting that the northern rivers may have had less of the more erosionally resistant lithology to erode through.

The present day rivers vary in potential erosional capacity based on modern precipitation patterns in the catchment areas, with higher rates in the north compared to the south (Garcia et al. 2011). Quebrada Lluta has a catchment with present-day precipitation rates of up to 200 mm/yr (Garcia et al. 2011). The catchments of Quebradas Azapa, Victor and Camarones have lower rates of 100 mm/yr (Garcia et al. 2011) and south of Quebrada Camarones the river catchments have rates of < 100 mm/yr (Garcia et al. 2011). Today, the lower precipitation rates to the south may mean that these rivers were slower to adapt to base-level change and potentially promote the apparent diachronous incision of the rivers within the Longitudinal Valley. However precipitation rates are likely to have varied in the past in response to Andean Uplift (Ehlers and Poulsen 2009). Also the configuration of the catchment areas of the individual rivers has varied through time. For example, Quebrada Azapa and Lluta drain through to higher precipitation regions through the Huaylillas Basin and Copaquilla Basin, respectively. The timing of when these rivers captured these basins can be constrained by when sedimentation in the two basins ceased, within the Huaylillas Basin between 5.7 Ma to 2.7 Ma and within the Copaquilla Basin from 10.7 Ma to 7.7 Ma. Prior to these capturing events both rivers would have been restricted to draining areas of precipitation rates < 100 mm/yr (based on modern precipitation values) similar to the southern rivers at this time. So the effect of precipitation variability with time is unclear.

The timing of the uplift of the Coastal Cordillera is poorly constrained and may have been highly diachronous from north to south in northern Chile (Mather and Hartley

2006, Madella et al. 2016). Melnick (2016) attributes coastal uplift to the transition between a shallow, locked seismogenic domain and a deeper region of modest seismicity. Around the Bolivian orocline uplift rates are lower compared to the Coastal Cordillera further to the north and south (Madella et al. 2016) suggesting that river systems may have drained from the Longitudinal Valley into the Pacific from 25 Ma (Madella et al. 2016). This interpretation is consistent with reconstruction of the paleotopography proximal to the Lluta Quebrada (van Zalinge et al. 2016b), which indicates that a deep paleovalley was already present in the Precordillera by ~23 Ma. Between ~23 and ~19 Ma, this region was covered by large-volume ignimbrites, restricting further sedimentation (van Zalinge et al. 2016b, Madella et al. 2016). Post-19 Ma, sedimentation continued to be absent between 18°10'S to 18°20'S (end of stratigraphic Unit 2). Between 19 and 10 Ma, first the Huaylillas then the Oxaya anticlines developed (Figure 3) in this region creating topographic barriers that trapped sediments in Precordilleran Basins to the east (e.g. Huaylas Formation from ~19 Ma within the Copaquilla Basin and from ~12 Ma in the Huaylillas Basin; Figure 15 and Garcia and Hérail, 2005). This restricted westward sediment transport from the Western Cordillera. Contemporaneously, a proto Lluta valley located in a similar location to the present day river was established and this drainage system bypassed the Longitudinal Valley depositing sediment generated in the Precordillera and Western Cordillera directly into the Pacific Ocean (Madella et al. 2016).

To the south of this region the uplift of the Coastal Cordillera was rapid enough to provide a substantial barrier to westward flowing fluvial systems. The Longitudinal Valley was a major depocentre after 23 Ma, while the Coastal Cordillera became a watershed with drainage systems into the Pacific being restricted to the coastal (western) slopes. Variations in relative base level driven by the interaction of global sea-level changes with relative uplift of the cordillera could have propagated up the drainage systems along the coast leading to headward erosion and incision facilitated during more humid periods. Given sufficient time, headward erosion would eventually result in incision through the Coastal Cordillera at the narrowest and lowest points (in the north), capturing fluvial systems in the Longitudinal Valley

and propagating through to the Precordillera. Once the Coastal Cordillera was breached and linked though to the Precordillera it would generate a fully incised network, which is more efficient at downcutting (due to the confined nature of the flows) than the adjacent distributive fluvial systems. As soon as substantive incision was established any future sediment and water discharge variations related to climate or tectonic change would be routed down these pre-existing valleys, bypassing the older paleosurface in the local area. This spatial variation in river incision associated with the width and height of the Coastal Cordillera would lead to a diachronous shift in endorheic to exorheic (drainage) and deposition (stratigraphic units) through the region from north to south. This interpretation is supported by deposition of stratigraphic Units 3 and 4 which are increasingly restricted to the southern part of the study area as Quebradas Lluta, Victor and Camarones incised through the Coastal Cordillera and Longitudinal Valley and captured sediments generated in the Precordillera between ~15 Ma and ~11 Ma. The final northern river to incise was Quebrada Tana at ~6.4 Ma (Hoke et al. 2007) although the further to the south the Rio Loa incised as late as 3 Ma (Hartley et al. 2000).

5.3 Tectonic Controls on the formation of the PPS

Tectonic processes are a major factor in the formation of the PPS. At a large scale Andean uplift related to changes in the plate convergence rate was a key control. Deformation associated with the uplift of the Andes has generated discrete morphotectonic provinces (Figure 1) bounded by major fault systems (Allmendinger et al. 1997). The PPS development involves four of these provinces; the Coastal Cordillera, Longitudinal Valley, Precordillera and Western Cordillera. The Coastal Cordillera acts as a barrier to sediment transport to the ocean, trapping sediment in the Longitudinal Valley in Regions 2 and 3. The Western Cordillera is a sediment source and the water shed for the major drainage networks. The Precordillera is a province characterised by both degradational and aggradational surfaces whereas the Longitudinal Valley forms the main depocentre. The relative uplift or subsidence of each of these provinces has had an effect on the development of the PPS.

Increased convergence in the Oligocene leading to crustal shortening and thickening spawned the most recent major episode of uplift of the Andes (Figure 14).

From the late Oligocene to the present day the Andes has generated sediment supplied from the east. The Coastal Cordillera, which initially formed from a major episode of uplift and exhumation in the Eocene (Juez-Larre et al. 2010), has continued to uplift in areas to the north and south of the Bolivian orocline (Madella et al. 2016). These tectonic processes resulted in the Longitudinal Valley being developed from the Late Oligocene, providing a major depocentre for sediments. Superimposed on this broader tectonic evolution are the more local manifestations of shortening and uplift across the Precordillera, which have tilted and folded the older surfaces, for example along the AdP basement high. Fold development north of 19°S formed local depocentres between the Precordillera and Western Cordillera and restricted sediment supply to the Longitudinal Valley (Garcia and Hérail, 2005; van Zalinge et al., 2016b).

Elevation profiles through the Longitudinal Valley, constructed from the DEM, constrain areas of relative uplift. The large-scale tectonic control is illustrated by the longitudinal variations in the altitude of the PPS (Figure 7). Using these profiles, we have identified three morphologically contrasting regions of the PPS that reflect different tectonic controls.

Region 1 (17°30'S-19°20'S) drains to the Pacific and there is a large elevation difference between the eastern (a-a') and western (b-b') edge of the Longitudinal Valley, leading to a net degradational landscape. The altitude of the PPS in the east is over 1000 m lower than in Region 2 and the Coastal Cordillera becomes subdued and even disappears between 18◦4'S and 18◦1'S (Figure 7). Incision has resulted in river capture of sediment from the Western Cordillera and focused drainage across the Longitudinal Valley to the Pacific Ocean such that sedimentary units are either absent (stratigraphic units 3-6 in Region 1) or greatly reduced in thickness (with the exception of the late Oligocene and early Miocene Azapa Formation). These

processes have led to a largely erosive landscape in Region 1 with young exposure ages.

On average, up to 250 m thickness of Aggradation Surface 4 has been eroded from the eastern edge of the PPS within Region 1 (Figure 7). The amount of incision varies spatially depending on river system connection to sea level, relative uplift of the area, and regional climate. The degradational surfaces in this region can be shown to be long-lived (millions of years) with multiple stages of development. For example, the paleo-Quebrada Lluta had already incised by ~23 Ma (van Zalinge et al. 2016b) in a similar location to the present day valley. Since this time, degradational surfaces (DS2 and DS3) also formed contemporaneously on the upper paleosurface. The trellis drainage of DS2 is constrained as forming before 11 ± 0.6 Ma by the Marquez lavas that infill the drainage (García et al. 2011), and remained active until it was largely abandoned at ~3 Ma. Taken together, the observations indicate episodic deposition and erosion with the latter resulting in degradational surface development and deep incision.

Region 2 (19°20'S-21°00'S) is predominantly internally drained and shows higher elevations of ~2200 m along the eastern edge of the Longitudinal Valley compared to Regions 1 and 3 (Figure 7). This topographic high corresponds to the widest segment of the Andean range and to the part of the Altiplano underlain by a high velocity zone in the upper mantle (Barnes and Ehlers, 2009). The Coastal Cordillera was elevated and the Longitudinal Valley was well developed, likely from around 23 Ma, such that the Longitudinal Valley has created a sizeable depocentre, enabling the preservation of major sedimentary units (Figure 9). The region can be divided into two basins south of 19°50'S, separated by a fault-controlled basement high in the subsurface (the Altos de Pica basement high; Jordan et al. 2010). The high elevation difference of ~1100 m from the east to west side of the Longitudinal Valley and enclosure of the basin to the west by the Coastal Cordillera has led to net aggradation in the west and net degradation in the east of the basin. This has led to preservation of the widest variation of paleosurfaces and the oldest exposure ages.

Region 3 (21°00'S-22°20'S) shows a decrease in the width of the Longitudinal Valley from 60 km to 30 km as the western basin in Region 2 pinches out with Region 3 hosting only the eastern basin. The elevation along the eastern side of the Longitudinal Valley decreases over 600 m from Region 2 to Region 3 whereas there is a slight increase in the elevation along the western edge leading to a small elevation difference (700 m to ~500 m) across the Valley. The Coastal Cordillera remains prominent such that the Longitudinal Valley acts as a major depocentre and forms a net aggradational system. The restricted accommodation space in the basin coupled with endorheic drainage results in a predominantly aggradational landscape with young apparent exposure ages.

These changes are clearly linked to the large-scale tectonic structures and processes. The three regions coincide closely with the main Altiplano plateau in the east (19°S to 23°S) and the presence of the Altiplano-Puna magma body (Chmielowski et al. 1999; Perkins et al. 2016), whereas the Altiplano-Puna region at about 4 km elevation extends from about 12°S to 32°S (Lamb and Davis, 2003). Region 1 is at the northern end of the Altiplano Plateau and coincides with the Bolivian Orocline, whereas to the south Region 3 is at the southern margin of main Altiplano plateau and just north of a region of more complex tectonics. Thus the north-south variations in the elevation of the PPS are inferred to be closely linked with processes involved in the formation of the Altiplano plateau. One view is that uplift is related to shear stress forces along the subducting plate interface (e.g. Lamb, 2000; Lamb and Davis, 2003). Another contribution to uplift might be isostatic adjustments due to igneous additions to the crust (Petford et al. 1996; Perkins et al. 2016). In the former case subduction interface shear stress may be linked to processes of tectonic erosion and role of subducted sediment (Lamb and Davis, 2003). In the latter case magmatic additions to the crust should be proportional to convergence rate and time. Perkins et al. (2016) developed a model in which formation of the Altiplano-Puna Magma Body (APMB) leads to uplift of up to 1.5 km since 11 Ma. Our observations thus support the hypothesis of Perkins et al. (2016) that regional uplift associated with emplacement of the APMB has caused deformation of the PPS to create the observed longtitudinal topographic profiles.

Recent events in all the morphotectonic units that have affected the PPS can be plausibly linked to the uplift of the Altiplano related to the emplacement of the AMPB, inducing uplift in the forearc in the 11 to 0 Ma period. However, the PPS history extends back much further to 19 Ma and the Tarapaca Paleosurface to 23 Ma. There is evidence of a major magmatic arc, deformation and uplift in the early to middle Miocene with some of the same drainage systems already being in existence (van Zaligne et al. 2017).

5.4 Climatic controls on the formation of the PPS

Superimposed on tectonic controls are the effects of changing climate which dictate precipitation rates and the geomorphological processes that govern landscape evolution and sediment transport (e.g. Mather et al 2014). Lamb and Davis (2003) have proposed that uplift may be regulated by climate in the Andes with increased aridity leading to larger subduction interface shear stresses. The regional hiatuses suggest a background climate of hyper-aridity since the early Miocene, which episodically switched to relatively more humid (but still arid) conditions at ~35-23 Ma, ~18-13 Ma, 12-11 Ma, 8-7 Ma and 5-3 Ma. This is in agreement with compositional variations in the soil in northern Chile between 21°S to 22°S that suggest short-lived humid intervals (~1 m.y. or less) with hyperarid periods persisting for longer time periods (1-5 m.y.; Jordan et al. 2014; Figure 14). The background hyperaridity in the region can be extended back as far as the late Oligocene in agreement with surface exposure ages in the Coastal Cordillera (Dunai et al. 2005; Kober et al. 2007).

During humid (but still arid) phases increased water and sediment discharge into the Longitudinal Valley would have led to large scale reduction in relief of the PPS by aggradation or degradation processes. In areas where the Longitudinal Valley is under net degradation (erosion) due to relatively lower base levels (exorheic drainage to the Pacific) and/or high elevation differences across the basin, the landscape would have formed a series of large drainage networks that erode into

and truncate the older stratigraphy. In areas where the Longitudinal Valley is under net aggradation due to higher base levels (endorheic drainage into the Longitudinal Valley) and low accommodation space, a series of distributive fluvial system deposits are preserved forming the stratigraphic units. Thus erosion and deposition surfaces occur contemporaneously in different areas. During drier (hyper-arid) phases, water and sediment discharge decrease, leading to contraction of active catchment areas and drainage routing confined to the pre existing valleys leading to abandonment of older regionally extensive paleosurfaces (both aggradational and degradational).

The time period between humid phases (millions of years), coupled with the arid climate, is sufficient to allow tectonic activity to alter the geomorphological framework of the region. The sediment sinks shift in response to the tectonically-modified geomorphology such that subsequent sedimentary units are developed and preserved in different locations to previous units. For example, deposition of stratigraphic units 3-4 occurred within the center of the Longitudinal Valley with subsequent deposition of stratigraphic unit 5 restricted to the western edge of the valley. The region represents a unique landscape due to the extreme long-term hyperaridity that results in tectonic activity outpacing sediment accumulation.

Climate change in the region over the last 25 million years could be affected by both global processes and local changes related to, for instance, the uplift of the Andes. In order to determine the relative significance of the two, local climate signatures can be compared to global Cenozoic climate trends recorded by $\delta^{18}O$ and $\delta^{13}C$ deep sea isotope records (Figure 14).

The oldest shift to hyperaridity constrained by this study occurred at the end of the Oligocene (~23 Ma) and can be related to the formation of the Tarapaca Paleosurface in the Coastal Cordillera. The shift coincides with a rapid increase in global temperature followed by a brief period of global cooling (Figure 14 and Zachos et al. 2001). Contemporaneously the circum-polar current was established and intensified (Frakes et al. 1992; Zachos et al. 2001; Houston and Hartley 2003). Increased high latitude oceanic circulation would have cooled polar waters around

Antarctica decreasing the temperature of the upwelling Humboldt Current along the west coast of South America suppressing the evaporation of moist air masses that could be transported inland.

During the Early Miocene, oxygen and carbon isotope signatures remained relatively constant until the Mid-Miocene Climatic Optimum at 15-13 Ma (Frakes et al. 1992 and Zachos et al. 2001). At this time a rapid period of cooling is recorded at higher latitudes associated with the build up of permanent East Antarctic ice sheets and increasingly arid conditions at lower latitudes (Frakes et al. 1992, Zachos et al. 2001), suggesting that this glacial climatic rearrangement increased aridity along the western escarpment of the Andes.

Aggradational Surface 4 formed at ~10 Ma. This correlates with cooling of the sub-Antarctic region (Lawver et al. 1992) and decreasing global temperatures. Surface 3 formed at ~7 Ma, at a time when the Southern Ocean upper circum-polar and intermediate water masses cooled (Billups et al. 2002). At this time, along the west coast of South America, increased glaciation occurred within the Patagonian Mountains (Frakes et al. 1992).

Surface 2 formed at ~3 Ma, corresponding to the closure of the Central American Seaway, which shut off flow between the Atlantic and Pacific Ocean and reorganised surface circulation (Molina-Cruz 1997; Huag and Tiedemann 1998) increasing the strength of the Peru counter current. This time period also correlates with the final humid phase along the western flank of South America before the climate reverted back to its present day hyperarid state.

5.5 Evolution of the PPS

Uplift of the Andes is thought to have initiated in the late Eocene with sediments shedding off the emerging mountain range during the Oligocene (Wörner et al. 2002), infilling the Longitudinal Valley and paleo-basins within the Coastal Cordillera under an arid to semi-arid regime (Figure 15A; Hartley and Evenstar 2010). At ~23

Ma, uplift of the Coastal Cordillera trapped sediments within the Longitudinal Valley and preserved the Coastal Tarapaca Surface as a relict paleosurface (Figure 15B). From 23 Ma to 19 Ma, a sequence of ~1000 m-thick ignimbrites covered the region between 17°S to 19°S (Figure 15D), interfingering with sediments north and south of this area. At ~19 Ma the Coastal Cordillera continued to uplift, restricting accommodation space to the centre of the Longitudinal Valley and preserving AS5 in the west. At around 17-16 Ma, the climate had become more humid with deposition of stratigraphic Unit 3 within the centre and eastern edge of the Longitudinal Valley (Figure 15C). Quebradas Azapa, Victor and Camarones incised the Longitudinal Valley, restricting sedimentation in the Longitudinal Valley to the south of 19◦2'S. In the Mid-Miocene (13-12 Ma) the climate reverted back to hyperaridity with a regional hiatus in sedimentation before a brief humid period recorded by deposition of stratigraphic Unit 4 in the late mid-Miocene. At ~11 Ma the climate became more arid again, forming AS4.

Between 11 Ma and 8 Ma, uplift of the Precordillera and Western Cordillera occurred relative to the Coastal Cordillera, creating accommodation space on the western side of the AdP basement high in Region 2 and across the valley in Region 3. In Region 1, base levels remained low as the region was externally drained such that an incisional, degradation network formed on the eastern side of the Longitudinal Valley. At ~8 Ma there was a shift to more humid conditions with the development of a regionally extensive degradational surface in Region 1 and the eastern edge of Region 2, and a series of large distributive fluvial systems in Region 3 and the western edge of Region 2 (Figure 15F). At ~7 Ma the climate reverted back to hyperaridity preserving AS3 and DS3.

At 5 Ma the climate became more humid, increasing rainfall and sediment discharge, which in turn would have enhanced incision rates in pre-existing drainages such as the Rio Loa through the Coastal Cordillera (Hartley et al. 2000). A regionally extensive drainage network (DS2) formed in Region 1 and the eastern edge of Region 2, and a series of large distributive fluvial systems (AS2) in Region 3 and the western edge of Region 2. At ~3 Ma the climate reverted back to hyperarid, preserving AS2

and DS2. These surfaces can be correlated through to the relict paleosurfaces identified by Placzek et al. (2010) in the Pre-Andean Basins (Figure 1A).

The post-Pliocene climate has been dominantly hyperarid with numerous short-lived relatively more humid periods, though much smaller in magnitude than the older events (Jordan et al. 2014). Between 21°S and 20°S sedimentation is restricted to thin lobe development on the northern tip of older distributive fluvial systems (Figure 15H). North of 20°S, later humid events are restricted to increased flow within the five main Quebradas (Incisional Drainage Network (IDN1)).

6. Conclusion

The PPS is a complex regionally extensive surface formed at a classic destructive plate margin. The extreme aridity has resulted in the preservation of ancient landscape components such that it provides a unique opportunity to examine Earth surface processes on geologic time-scales, without the complications introduced by vegetation control on sediment supply and hillslope hydrology. Consequently tectonic activity outpaces sediment accumulation providing a record of how the uplift of the main morphotectonic provinces of a mountain belt has evolved over millions of years. In this study, we have re-examined the PPS between 18°S and 22°S, compiled existing work on the underlying geology, sedimentology, surface dating and seismic profiling and combined it with new multispectral satellite maps and 45 new cosmogenic ^{3}He and ^{21}Ne surface exposure ages. The principal conclusions are:

1. The Pacific Paleosurface is a complex paleosurface that has been formed over at least 5 distinct periods of aggradation and degradation of fluvial systems. It overlaps the Longitudinal Valley, stretching for 800 km from southern Peru into northern Chile.
2. The distinct surfaces yield markedly different cosmogenic nuclide surface exposure ages (which are coherent with bracketing Ar/Ar ages) that are

consistent with formation at approximately 23 Ma, 19 Ma, 11 Ma, 7 Ma and 3 Ma.

3. The data support evidence for a dominantly hyperarid climate since at least 25 Ma (Dunai et al. 2005), which switched episodically to relatively more humid (but still arid) conditions at 35-23 Ma, 18-13 Ma, 12-11 Ma, 8-7 Ma and 5-3 Ma. Increased sediment discharge into the Longitudinal Valley during these more humid phases led to large scale reduction of relief of the PPS by aggradational or degradational processes. An absence of sediment discharge during the hyper-arid phases led to contraction of active catchments with sediment routing confined to pre-existing valleys, which led to abandonment of the older, regionally extensive paleosurfaces (both aggradational and degradational).

4. The timing of the formation of the individual surface of the PPS appears to be related to regional climate changes, whereas the location of the surfaces is controlled by regional and local tectonic activity.

5. Two main factors control the deposition and preservation of the stratigraphic units and paleosurfaces throughout the Longitudinal Valley: (1) shifts in accommodation space related to uplift of the Coastal Cordillera vs. the Precordillera; and (2) diachronous river capture.

6. The PPS can be divided into 3 distinct regions on the basis of surface formation and preservation. Regions 1 and 2 are present in the wide Longitudinal Valley and have large differences in elevation between the Coastal Cordillera and Precordillera. Regions 2 and 3 have endorheic drainage whereas Region 1 is controlled by diachronous river capture. These variations have led to different phases of paleosurface formation across the regions. Region 1 is dominantly a degradational landscape, whereas Region 3 is dominated by an aggradational landscape. Region 2 shows a combination of both aggradation and degradation, leading to preservation of the widest range of paleosurfaces from Early Miocene to the present day.

7. The deposition and preservation of sediments in the Longitudinal Valley since ~35 Ma suggest that the Andes have been a major sedimentary source since at least the Late Oligocene.

.

7. Acknowledgements

This study was funded by BHP Billiton. The authors are grateful to Marit Van Zalinge for discussion in the field, Luigia Di Nicola and Ana Caracedo for assistance in the noble gas laboratory at SUERC and Brian Tattitch for helpful discussions on the paper. We are grateful to Simon Lamb and an anonymous review whose contributions significantly improved the manuscript.

References

Al-Farraj, A. and Harvey, A.M., 2000. Desert pavement characteristics on wadi terrace and alluvial fan surfaces: Wadi Al-Bih, UAE and Oman. Geomorphology, 35(3): 279-297.

Allmendinger, R.W., Jordan, T.E., Kay, S.M. and Isacks, B.L., 1997. The evolution of the Altiplano-Puna plateau of the Central Andes. Annual Review of Earth and Planetary Sciences, 25: 139-174.

Allmendinger, R.W., Gonzalez,G., Yu, J., Hoke, G. and Isacks, B., 2005. Trench-parallel shortening in the Northern Chilean Forearc: Tectonic and climatic implications. Geological Society of America Bulletin, 117: 89-104.

Alpers, C.N. and Brimhall, G.H., 1988. Middle Miocene Climatic-Change in the Atacama Desert, Northern Chile - Evidence from Supergene Mineralization at La-Escondida. Geological Society of America Bulletin, 100(10): 1640-1656.

Alván, A., von Eynatten, H., Dunkl, I. and Gerdes, A., 2015. Zircon U–Pb geochronology and heavy mineral composition of the Camaná Formation, southern Peru: Constraints on sediment provenance and uplift of the Coastal and Western Cordilleras. Journal of South American Earth Sciences, 61: 14-32.

Anton, L., Mather, A., Stokes, M., Muñoz-Martin, A. and De Vicente, G., 2015. Exceptional river gorge formation from unexceptional floods. Nature Communications, 6(7963): 1-11.

Armijo, R., Lacassin, R., Coudurier-Curveur, A. and Carrizo, D., 2015. Coupled tectonic evolution of Andean orogeny and global climate. Earth-Science Reviews, 143: 1-35.

Arriagada, C., Roperch, P., Mpodozis, C. and Cobbold, P., 2008. Paleogene building of the Bolivian Orocline: Tectonic restoration of the central Andes in 2-D map view. Tectonics, 27(6): TC6014.

Balco, G. and Shuster, D.L., 2009. Production rate of cosmogenic 21 Ne in quartz estimated from ^{10}Be, ^{26}Al, and ^{21}Ne concentrations in slowly eroding Antarctic bedrock surfaces. Earth and Planetary Science Letters, 281(1): 48-58.

Balco, G., Stone, J.O., Lifton, N.A. and Dunai, T.J., 2008. A complete and easily accessible means of calculating surface exposure ages or erosion rates from ^{10}Be and ^{26}Al measurements. Quaternary geochronology, 3(3): 174-195.

Barke, R. and Lamb, S., 2006. Late Cenozoic uplift of the Eastern Cordillera, Bolivian Andes. Earth and Planetary Science Letters, 249(3-4): 350-367.

Barker, P. and Burrell, J., 1977. The opening of Drake passage. Marine geology, 25(1): 15-34.

Barnes, J.B. and Ehlers, T.A., 2009. End member models for Andean Plateau uplift. Earth-Science Reviews, 97(1-4): 105-132.

Billups, K., 2002. Late Miocene through early Pliocene deep water circulation and climate change viewed from the sub-Antarctic South Atlantic. Palaeogeography, Palaeoclimatology, Palaeoecology, 185(3): 287-307.

Blard, P.H., Lavé, J., Sylvestre, F., Placzek, C.J., Claude, C., Galy, V., Condom, T. and Tibari, B., 2013. Cosmogenic ^{3}He production rate in the high tropical Andes (3800 m, 20°S): Implications for the local last glacial maximum. Earth and Planetary Science Letters, 377–378: 260-275.

Bull, WB. 1977. Tectonic Geomorphology of the Mojave Desert. USGS report 14-08-001-G-394. Menlo Park CA: Office of Earthquakes, Volcanoes and Engineering.

Capitanio, F., Faccenna, C., Zlotnik, S. and Stegman, D., 2011. Subduction dynamics and the origin of Andean orogeny and the Bolivian orocline. Nature, 480(7375): 83-86.

Charrier, R., Hérail, G., Pinto, L., García, M., Riquelme, R., Farías, M. and Muñoz, N., 2012. Cenozoic tectonic evolution in the Central Andes in northern Chile and west central Bolivia: implications for paleogeographic, magmatic and mountain building evolution. International Journal of Earth Sciences, 102(1): 235-264.

Chmielowski, J., Zandt, G. and Haberland, C., 1999. The central Andean Altiplano-Puna magma body. Geophysical Research Letters, 26(6): 783-786.

Codilean, A.T., Bishop, P., Stuart, F.M., Hoey, T., Fabel, D. and Freeman SPHT., 2008. Single-grain cosmogenic Ne-21 concentrations in fluvial sediments reveal spatially variable erosion rates, Geology 36(1): 159-162.

Cooper, F.J., Adams, B.A., Blundy, J.D., Farley, K.A., McKeon, R.E., Ruggiero, A., 2016. Aridity-induced Miocene canyon incision in the Central Andes, Geology 44(8): 675-678.

Dauncey, P. and Coop, M.R., 2012. Engineering behaviour of desert soils. Geological Society, London, Engineering Geology Special Publications, 25(1): 259-299.

Decou, A., Von Eynatten, H., Mamani, M., Sempere, T. and Wörner, G., 2011. Cenozoic forearc basin sediments in Southern Peru (15–18°S): Stratigraphic and heavy mineral constraints for Eocene to Miocene evolution of the Central Andes. Sedimentary Geology, 237(1): 55-72.

Delouis, B., Philip, H., Dorbath, L. and Cisternas, A., 1998. Recent crustal deformation in the Antofagasta region (northern Chile) and the subduction process. Geophysical Journal International, 132(2): 302-338.

Dunai, T.J., Gonzalez-Lopez, G.A., Juez-Larre, J. and Carrizo, D., 2005. Preservation of (early) miocence landscapes in the Atacama Desert, northern Chile. Geochimica Et Cosmochimica Acta, 69(10): A161-A161.

Ewing, S.A., Sutter, B., Owen, J., Nishiizumi, K., Sharp, W., Cliff, S.S., Perry, K., Dietrich, W., McKay, C.P. and Amundson, R., 2006. A threshold in soil formation at Earth's arid–hyperarid transition. Geochimica et Cosmochimica Acta, 70(21): 5293-5322.

Ehlers, T.A. and Poulsen, C.J., 2009. Influence of Andean uplift on climate and paleoaltimetry estimates. Earth and Planetary Science Letters, 281(3-4): 238-248.

Evenstar, L.A., Hartley, A.J., Archer, S.G. and Neilson, J.E., 2015. Climatic and halokinetic controls on alluvial–lacustrine sedimentation during compressional deformation, Andean forearc, northern Chile. Basin Research 28: 634-657.

Evenstar, L.A., Hartley, A.J., Stuart, F.M., Mather, A.E., Rice, C.M. and Chong, G., 2009. Multiphase development of the Atacama Planation Surface recorded by cosmogenic He-3 exposure ages: Implications for uplift and Cenozoic climate change in western South America. Geology, 37(1): 27-30.

Evenstar, L.A., Stuart, F.M., Hartley, A.J. and Tattitch, B., 2015. Slow Cenozoic uplift of the western Andean Cordillera indicated by cosmogenic 3He in alluvial boulders from the Pacific Planation Surface. Geophysical Research Letters, 42(20): 8448-8455.

Farías, M., Charrier, R., Comte, D., Martinod, J. and Hérail, G., 2005. Late Cenozoic deformation and uplift of the western flank of the Altiplano: Evidence from the depositional, tectonic, and geomorphologic evolution and shallow seismic activity (northern Chile at 19°30'S). Tectonics, 24(4): TC4001.

Foeken, J.P.T., S Day, S., Stuart, F.M., 2009. Cosmogenic 3He exposure dating of the Quaternary basalts from Fogo, Cape Verdes: implications for rift zone and magmatic reorganisation. Quaternary Geochronology 4(1): 37-49.

Foeken, J.P.T., Stuart, F.M. and Mark, D.F., 2012. Long-term low latitude cosmogenic He-3 production rate determined from a 126 ka basalt from Fogo, Cape Verdes. Earth and Planetary Science Letters, 359: 14-25.

Frakes, L.A., Francis, J.E. and Syktus, J.I., 2005. Climate modes of the Phanerozoic. Cambridge University Press.

Galli-Olivier, C., 1967. Pediplain in Northern Chile and the Andean Uplift. Science, 158(3801): 653-655.

Galli, C., 1968. Cuadrángulo Juan de Morales, Provincia de Tarapacá. Instituto de Investigaciones Geológicas, Carta Geológica de Chile, 18, scale 1:50.000.

Garcia, M. and Herail, G., 2005. Fault-related folding, drainage network evolution and valley incision during the Neogene in the Andean Precordillera of Northern Chile. Geomorphology, 65(3-4): 279-300.

Garcia, M., Riquelme, R., Farias, M., Herail, G. and Charrier, R., 2011. Late Miocene-Holocene canyon incision in the western Altiplano, northern Chile: tectonic or climatic forcing? Journal of the Geological Society, 168(4): 1047-1060.

Garzione, C.N., Hoke, G.D., Libarkin, J.C., Withers, S., MacFadden, B., Eiler, J., Ghosh, P. and Mulch, A., 2008. Rise of the Andes. Science, 320(5881): 1304-7.

Garzione, C.N., Molnar, P., Libarkin, J.C. and MacFadden, B.J., 2006. Rapid late Miocene rise of the Bolivian Altiplano: Evidence for removal of mantle lithosphere. Earth and Planetary Science Letters, 241(3-4): 543-556.

Gaupp, R., Kött, A. and Wörner, G., 1999. Palaeoclimatic implications of Mio–Pliocene sedimentation in the high-altitude intra-arc Lauca Basin of northern Chile. Palaeogeography, Palaeoclimatology, Palaeoecology, 151(1): 79-100.

Ghosh, P., Garzione, C.N. and Eiler, J.M., 2006. Rapid uplift of the Altiplano revealed through C-13-O-18 bonds in paleosol carbonates. Science, 311(5760): 511-515.

Goehring, B.M., Kurz, M.D., Balco, G., Schaefer, J.M., Licciardi, J. and Lifton, N., 2010. A re-evaluation of in situ cosmogenic He-3 production rates. Quaternary Geochronology, 5(4): 410-418.

Gosse, J.C. and Phillips, F.M., 2001. Terrestrial in situ cosmogenic nuclides: theory and application. Quaternary Science Reviews, 20(14): 1475-1560.

Guo, Z., Ruddiman, W.F., Hao, Q., Wu, H., Qiao, Y., Zhu, R.X., Peng, S., Wei, J., Yuan, B. and Liu, T., 2002. Onset of Asian desertification by 22 Myr ago inferred from loess deposits in China. Nature, 416(6877): 159-163.

Hartley, A.J. and May, G., 1998. Miocene gypcretes from the Calama Basin, northern Chile. Sedimentology, 45(2): 351-364.

Hartley, A.J., May, G., Chong, G., Turner, P., Kape, S.J. and Jolley, E.J., 2000. Development of a continental forearc: A Cenozoic example from the Central Andes, northern Chile. Geology, 28(4): 331-334.

Hartley, A.J. and Rice, C.M., 2005. Controls on supergene enrichment of porphyry copper deposits in the Central Andes: A review and discussion. Mineralium Deposita, 40(5): 515-525.

Hartley, A.J., Sempere, T. and Worner, G., 2007. A comment on "Rapid late Miocene rise of the Bolivian Altiplano: Evidence for removal of mantle lithosphere" by C.N.

Garzione et al. [Earth Planet. Sci. Lett. 241 (2006) 543-556]. Earth and Planetary Science Letters, 259(3-4): 625-629.

Hartley, A.J. and Evenstar, L., 2010. Cenozoic stratigraphic development in the north Chilean forearc: Implications for basin development and uplift history of the Central Andean margin. Tectonophysics, 495(1-2): 67-77.

Haug, G.H. and Tiedemann, R., 1998. Effect of the formation of the Isthmus of Panama on Atlantic Ocean thermohaline circulation. Nature, 393(6686): 673-676.

Hoke, G.D., Isacks, B.L., Jordan, T.E., Blanco, N., Tomlinson, A.J. and Ramezani, J., 2007. Geomorphic evidence for post-10 Ma uplift of the western flank of the central Andes 18°30′-22°S. Tectonics, 26(5): TC5021.

Hoke, G.D. and Garzione, C.N., 2008. Paleosurfaces, paleoelevation, and the mechanisms for the late Miocene topographic development of the Altiplano plateau. Earth and Planetary Science Letters, 271(1-4): 192-201.

Houston, J. and Hartley, A.J., 2003. The central Andean west-slope rainshadow and its potential contribution to the origin of hyper-aridity in the Atacama Desert. International Journal of Climatology, 23(12): 1453-1464.

Isacks, B.L., 1988. Uplift of the Central Andean Plateau and Bending of the Bolivian Orocline. Journal of Geophysical Research-Solid Earth and Planets, 93(B4): 3211-3231.

Jordan, T.E., Isacks, B.L., Allmendinger, R.W., Brewer, J.A., Ramos, V.A. and Ando, C.J., 1983. Andean Tectonics Related to Geometry of Subducted Nazca Plate. Geological Society of America Bulletin, 94(3): 341-361.

Jordan, T.E., Nester, P.L., Blanco, N., Hoke, G.D., Davila, F. and Tomlinson, A.J., 2010. Uplift of the Altiplano-Puna plateau: A view from the west. Tectonics, 29; TC5007.

Jordan, T.E., Kirk-Lawlor, N.E., Blanco P., N., Rech, J.A. and Cosentino, N.J., 2014. Landscape modification in response to repeated onset of hyperarid paleoclimate states since 14 Ma, Atacama Desert, Chile. Geological Society of America Bulletin 94: 341-361.

Jordan, T., Herrera Lameli, C., Kirk-Lawlor, N. and Godfrey, L., 2015. Architecture of the aquifers of the Calama Basin, Loa catchment basin, northern Chile. Geosphere 11(5): 1-38.

Juez-Larré, J., Kukowski, N., Dunai, T.J., Hartley, A.J. and Andreissen, P.A.M. 2010. Thermal and exhumation history of the Coastal Cordillera arc of northern Chile revealed by thermochronological dating. Tectonophysics, 495: 48-66.

Jungers, M.C., Heimsath, A.M., Amundson, R., Balco, G., Shuster, D. and Chong, G., 2013. Active erosion–deposition cycles in the hyperarid Atacama Desert of Northern Chile. Earth and Planetary Science Letters, 371: 125-133.

Kennan, L., Lamb, S. and Rundle, C., 1995. K-Ar Dates from the Altiplano and Cordillera-Oriental of Bolivia - Implications for Cenozoic Stratigraphy and Tectonics. Journal of South American Earth Sciences, 8(2): 163-186.

Kiefer, E., Dorr, M.J., Ibbeken, H. and Gotze, H.-J., 1997. Gravity-based mass balance of an alluvial fan giant: the Arcas Fan, Pampa del Tamarugal, Northern Chile. Andean Geology, 24(2): 165-185.

Kober, F., Ivy-Ochs, S., Schlunegger, F., Baur, H., Kubik, P.W. and Wieler, R., 2007. Denudation rates and a topography-driven rainfall threshold in northern Chile: Multiple cosmogenic nuclide data and sediment yield budgets. Geomorphology, 83(1-2): 97-120.

Kött, A., Gaupp, R. and Wörner, G., 1995. Miocene to Recent history of the Western Altiplano in Northern Chile revealed by lacustrine sediments of the Lauca Basin (18 15'–18 40' S/69 30'–69 05' W). Geologische Rundschau, 84(4): 770-780.

Lal, D., 1991. Cosmic ray labeling of erosion surfaces: in situ nuclide production rates and erosion models. Earth and Planetary Science Letters, 104(2–4): 424-439.

Lamb, S. and Hoke, L., 1997. Origin of the high plateau in the Central Andes, Bolivia, South America. Tectonics, 16(4): 623-649.

Lamb, S. and Davis, P., 2003. Cenozoic climate change as a possible cause for the rise of the Andes. Nature, 425(6960): 792-797.

Lamb, S. 2016. Cenozoic uplift of the Central Andes in northern Chile and Bolivia – reconciling paleoaltimetry with the geological evolution. Canadian Journal of Earth Sciences, 53(11): 1227-1245.

Lawver, L.A., Gahagan, L.M. and Coffin, M.F., 1992. The development of paleoseaways around Antarctica. The Antarctic Paleoenvironment: A Perspective on Global Change: Part One: 7-30.

Lear, C.H., Elderfield, H. and Wilson, P., 2003. A Cenozoic seawater Sr/Ca record from benthic foraminiferal calcite and its application in determining global weathering fluxes. Earth and Planetary Science Letters, 208(1): 69-84.

Lifton, N., Sato, T. and Dunai, T.J., 2014. Scaling in situ cosmogenic nuclide production rates using analytical approximations to atmospheric cosmic-ray fluxes. Earth and Planetary Science Letters, 386(0): 149-160.

Lu, H., Wang, X. and Li, L., 2010. Aeolian sediment evidence that global cooling has driven late Cenozoic stepwise aridification in central Asia. Geological Society, London, Special Publications, 342(1): 29-44.

Madella, A., Delunel, R., Audin, L. and Schlunegger, F., 2016. Why is there no Coastal Cordillera at the Arica Bend (Western Central Andes)? Basin Research, 1–21,

Masarik, J., 2002. Numerical simulation of in-situ production of cosmogenic nuclides. Geochimica Et Cosmochimica Acta, 66(15A): A491-A491.

Mather, A., Stokes, M. and Griffiths, J., 2002. Quaternary landscape evolution: a framework for understanding contemporary erosion, southeast Spain. Land Degradation & Development, 13(2): 89-109.

Mather, A.E. and Hartley, A.J., 2006. The application of drainage system analysis in constraining spatial patterns of uplift in the Coastal Cordillera of northern Chile. Geological Society of America Special Papers, 398: 87-99.

Mather, A.E., Hartley, A.J & Griffiths, J.S. 2014. The giant coastal landslides of Northern Chile: tectonic and climate interactions on a classic convergent plate margin. Earth & Planetary Science Letters 388, 249-256

Mather, AE, Stokes, M, Whitfield, L. 2016. *In press*. River terraces and alluvial fans: the case for an integrated Quaternary fluvial archive. Journal of Quaternary Science Reviews.

Matmon, A., Quade, J., Placzek, C., Fink, D., Copeland, A., Neilson, J.W. and Team, A., 2015. Seismic origin of the Atacama Desert boulder fields. Geomorphology, 231: 28-39.

May, G., Hartley, A.J., Stuart, F.M. and Chong, G., 1999. Tectonic signatures in arid continental basins: an example from the Upper Miocene-Pleistocene, Calama Basin, Andean forearc, northern Chile. Palaeogeography Palaeoclimatology Palaeoecology, 151(1-3): 55-77.

May, G., Hartley, A.J., Chong, G., Stuart, F., Turner, P. and Kape, S.J., 2005. Oligocene to Pleistocene Lithostratigraphy of the Calama Basin, northern Chile. Revista geológica de Chile, 32(1): 33-58.

McFadden, L.D., Wells, S.G. and Jercinovich, M.J., 1987. Influences of eolian and pedogenic processes on the origin and evolution of desert pavements. Geology, 15(6): 504-508.

Melnick, D., 2016. Rise of the central Andean coast by earthquakes straddling the Moho. Nature Geoscience 6: 401-407.

Molina-Cruz, A., 1997. Closing of the Central American Gateway and its effects on the distribution of Late Pliocene radiolarians in the eastern tropical Pacific. Tectonophysics, 281(1): 105-111.

Molnar, P. and Garzione, C.N., 2007. Bounds on the viscosity coefficient of continental lithosphere from removal of mantle lithosphere beneath the Altiplano and Eastern Cordillera. Tectonics, 26(2): TC2013

Mortimer, C. and Saric, N., 1972. Landform evolution in the coastal region of Tarapacá Province, Chile. Revista Géomorphology Dynamics, 21: 162–170

Mortimer, C., 1973. The Cenozoic history of the southern Atacama Desert, Chile. Journal of the Geological Society, 129(5): 505-526.

Mortimer C., Farrar., and Saric N., 1974. K-Ar ages from tertiary lavas of the northernmost Chilean Andes. Geologische Rundschau, 63: 484 - 493.

Nishiizumi, K., Caffee, M.W., Finkel, R.C., Brimhall, G. and Mote, T., 2005. Remnants of a fossil alluvial fan landscape of Miocene age in the Atacama Desert of northern Chile using cosmogenic nuclide exposure age dating. Earth and Planetary Science Letters, 237(3–4): 499-507.

Noble, D.C., Sébrier, M., Megard, F. and McKee, E.H., 1985. Demonstration of two pulses of Paleogene deformation in the Andes of Peru. Earth and Planetary Science Letters, 73(2): 345-349.

Perkins, J.P., Ward, K.M., de Silva, S., Zandt,G., Beck, S.L. and Finnegan, N.J., 2016. Surface uplift in the Central Andes driven by growth of the Altiplano Puna Magma Body. Nature Communications 7:13185.

Petford, N., Atherton, M. and Halliday, A., 1996. Rapid magma production rates, underplating and remelting in the Andes: Isotopic evidence from northern-central Peru (9–11°S). Journal of South American Earth Sciences, 9(1): 69-78.

Pinto, L., Hérail, G., Charrier, R., 2004. Syntectonic sedimentation associated with Neogene structures in the Precordillera of Moquella Zone, Tarapacá (19°15'S, northern Chile). Revista Geólogica De Chile, 31: 19-44.

Placzek, C.J., Matmon, A., Granger, D.E., Quade, J. and Niedermann, S., 2010. Evidence for active landscape evolution in the hyperarid Atacama from multiple terrestrial cosmogenic nuclides. Earth and Planetary Science Letters, 295(1–2): 12-20.

Quang, C.X., Clark, A.H., Lee, J.K.W. and Hawkes, N., 2005. Response of supergene processes to episodic Cenozoic uplift, pedimeńt erosion, and ignimbrite eruption in the Porphyry Copper Province of southern Perú. Economic Geology, 100(1): 87-114.

Rackham L.J., 1973. Notes to Accompany Land Unit Geomorphology Description Card, Land Resources Division, Tolworth.

Rech, J.A., Currie, B.S., Michalski, G. and Cowan, A.M., 2006. Neogene climate change and uplift in the Atacama Desert, Chile. Geology, 34(9): 761-764.

Ritter, M. E. (2006), The Physical Environment: an Introduction to Physical Geography.

Roperch, P., Sempere, T., Macedo, O., Arriagada, C., Fornari, M., Tapia, C., García, M. and Laj, C., 2006. Counterclockwise rotation of late Eocene–Oligocene fore-arc deposits in southern Peru and its significance for oroclinal bending in the central Andes. Tectonics, 25(3): TC3010.

Sáez, A., Cabrera, L., Jensen, A. and Chong, G., 1999. Late Neogene lacustrine record and palaeogeography in the Quillagua-Llamara basin, Central Andean fore-arc (northern Chile). Palaeogeography Palaeoclimatology Palaeoecology, 151(1-3): 5-37.

Sáez, A., Cabrera, L., Garcés, M., van den Bogaard, P., Jensen, A. and Gimeno, D., 2012. The stratigraphic record of changing hyperaridity in the Atacama desert over the last 10 Ma. Earth and Planetary Science Letters, 355: 32-38.

Santiago, C.M. and Rendic, N.S., Cenozoic studies in northernmost Chile. Geologische Rundschau, 64(1): 395-420.

Schumm, S., 1993. River response to baselevel change: implications for sequence stratigraphy. The Journal of Geology 101(2): 279-294.

Segerstorm, K., 1963. Matureland of northern Chile and its relationship to ore deposits. Geological Society of America Bulletin, 74(4): 513-518.

Seong, Y.B., Dorn, R.I. and Yu, B.Y., 2016. Evaluating the life expectancy of a desert pavement. Earth-Science Reviews, 162: 129-154.

Somoza, R., 1998. Updated Nazca (Farallon) - South America relative motions during the last 40 My: implications for mountain building in the central Andean region. Journal of South American Earth Sciences, 11(3): 211-215.

Stone, J., 2007. Cosmogenic nuclide calibration - A progress report from the CRONUS project. Geochimica Et Cosmochimica Acta, 71(15): A976-A976.

Thomas, D., 1997. Arid zone geomorphology: process, form and change in drylands 2nd edition Wiley. Blackwell, Chichester.

Thouret, J.-C., Wörner, G., Gunnell, Y., Singer, B., Zhang, X. and Souriot, T., 2007. Geochronologic and stratigraphic constraints on canyon incision and Miocene uplift of the Central Andes in Peru. Earth and Planetary Science Letters, 263(3): 151-166.

Tosdal, R.M., Clark, A.H. and Farrar, E., 1984. Cenozoic polyphase landscape and tectonic evolution of the Cordillera Occidental, southernmost Peru. Geological Society of America Bulletin, 95(11): 1318-1332.

Van der Wateren, F.M. and Dunai, T.J., 2001. Late Neogene passive margin denudation history—cosmogenic isotope measurements from the central Namib desert. Global and Planetary Change, 30(3): 271-307.

Van Zalinge, M., Sparks, R., Cooper, F. and Condon, D., 2016a. Early Miocene large-volume ignimbrites of the Oxaya Formation, Central Andes. Journal of the Geological Society, *173*(5), 716-733.

Van Zalinge, M, Sparks, S, Evenstar, L, Cooper, F, Aslin, J & Condon, D, 2016b, Using ignimbrites to quantify structural relief growth and understand deformation processes: Implications for the development of the Western Andean Slope, northernmost Chile. Lithosphere, 8, L593-1.

Victor, P., Oncken, O. and Glodny, J., 2004. Uplift of the western Altiplano plateau: Evidence from the Precordillera between 20° and 21°S (northern Chile). Tectonics, 23(4): TC4004.

Vergara, H., Thomas, A., 1984. Hoja Collacagua, Región de Tarapacá, Servicio

Nacional de Geología y Minería, Carta Geológica de Chile, 59, scale 1:250.000.

Weissmann, G., Hartley, A., Nichols, G., Scuderi, L., Olson, M., Buehler, H. and Banteah, R., 2010. Fluvial form in modern continental sedimentary basins: Distributive fluvial systems. Geology, 38(1): 39-42.

Wells, S.G., McFadden, L.D. and Dohrenwend, J.C., 1987. Influence of late Quaternary climatic changes on geomorphic and pedogenic processes on a desert piedmont, eastern Mojave Desert, California. Quaternary Research, 27(2): 130-146.

Wood, Y., Graham, R. and Wells, S., 2005. Surface control of desert pavement pedologic process and landscape function, Cima Volcanic field, Mojave Desert, California. Catena, 59(2): 205-230.

Wörner, G., Uhlig, D., Kohler, I. and Seyfried, H., 2002. Evolution of the West Andean Escarpment at 18°S (N. Chile) during the last 25 Ma: uplift, erosion and collapse through time. Tectonophysics, 345(1–4): 183-198.

Wotzlaw, J.F., Decou, A., von Eynatten, H., Wörner, G. and Frei, D., 2011. Jurassic to Palaeogene tectono-magmatic evolution of northern Chile and adjacent Bolivia from detrital zircon U-Pb geochronology and heavy mineral provenance. Terra Nova, 23(6): 399-406.

Zachos, J., Pagani, M., Sloan, L., Thomas, E. and Billups, K., 2001. Trends, rhythms, and aberrations in global climate 65 Ma to present. Science, 292(5517): 686-693.

Figures

Figure 1. (A) Digital elevation model of the Central Andes showing the five morphotectonic provinces. CB: Calama Basin, SdA: Salar de Atacama. (B) Mapped extent of the two major paleosurfaces in the region: the older Tarapaca/Altos de Camilaca Paleosurface, which lies within the Coastal Cordillera and Precordillera (Mortimer and Saric 1972, Mortimer and Rendic 1975, Tosdal et al. 1984, Quang et al. 2005) and the younger Pampa Lagunas/Pacific Paleosurface, which lies predominantly within the Longitudinal Valley (Galli-Oliver 1967; Mortimer et al. 1974, Tosdal et al. 1984, Hoke et al. 2004, Quang et al. 2005). Locations of N-S and E-W stratigraphic transects through the Longitudinal Valley presented in Figures 3 and 8.

Figure 2. (A) Major rivers (quebradas) that cross-cut the PPS and flow to the Pacific Ocean are depicted in blue. Black lines a and b refer to the elevation profiles shown in Figure 7. Coloured lines 1–6 are the locations of topographic profiles shown in Figure 2B and 2C. (B) Longitudinal river profiles (solid lines) and paleosurfaces (dashed lines) in a series of E-W transects through northern Chile. Profiles of the four northernmost rivers (1-4) previously published by García et al. (2011). (C) N-S cross-sections across the four northernmost rivers proximal to the Coastal Cordillera.

Figure 3. E-W transects across the Longitudinal Valley (locations shown in Figure 1A). Sections T and U are compiled from reflective seismic data (Jordan et al., 2010). Section S and the western edge of section T are complied from field observations in this study. AF: Ausipar Fault, MA: Moquella Anticline, HA: Huaylillas Anticline, AdP BH: Altos de Pica Basement High.

Figure 4. (A) False colour satellite image of the PPS from Landsat 7 Enhanced Thematic Mapper data (Red: Band 7 (2.1-2.35 μm), Green: Band 4 (0.75-0.9 μm), Blue: Band 2 (0.53-0.61 μm)). Boxes denote the locations of field photographs B, C, G and cross section H. (B) A modern desert surface with clear fluvial channel bar and

swale features. (C) Well developed desert pavement illustrated by the homogeneous, closely packed mosaic of angular pebble to cobble sized rock fragments. (D) Desert varnish on a clast sitting on the old desert pavement. (E) >20 cm-thick gypcrete soil directly beneath the desert pavement. (F) Long-wavelength undulation of desert pavement due to variable inflation of the underlying gypcrete soil. (G) Old desert pavement where absence of clasts on the surface reveals the underlying gypcrete soil. (H) Cross-section through Quebrada Camarones based on field observations of the canyon walls, location shown in 4A. Cross section shows the stratigraphic relationship between basement outcrops, Azapa Formation, Oxaya Formation and El Diablo Formation. On the eastern side of the section, the El Diablo Formation shows syn-sedimentary deposition with growth of the Moquella Anticline. To the west, deposition of the same unit is restricted by movement on an east verging reverse fault proximal to the Coastal Cordillera. Between this east verging fault and the Coastal Cordillera, the Oxaya Formation outcrops at the surface.

Figure 5. False colour shortwave infrared Landsat 7 Enhanced Thematic Mapper (ETM+) satellite image of the PPS. Red: Band 7 (2.1-2.35 µm), Green: Band 4 (0.75-0.9 µm), Blue: Band 2 (0.53-0.61 µm). Sampling sites for cosmogenic nuclide surface exposure dating are shown in white.

Figure 6. (A) Spatial extent of the five surfaces that make up the PPS, defined by mapping and sedimentary analysis carried out in this study. The surfaces are divided up into three geographic regions, discussed in the text. **(B)** Elevation profile across Aggradational Surface 4 and Degradational Surfaces 2 and 3 at 18°45'S. Transect line shown in Figure 6A. Solid black line is the current topographic profile. Solid purple, orange and red line represents the top of Aggradational Surface 4, Degradational Surface 3 and Degradational Surface 2 respectively. Dashed lines show projected elevations of Surfaces 2, 3, and 4 by extending the topographic slope to the East, which have since been removed by erosion of the younger surfaces or networks.

Figure 7. N-S elevation profiles along the Longitudinal Valley as shown in Figure 2A compared with the width of the Coastal Cordillera over the same distance. Solid

black lines represent the present day surface elevation along each profile. Thick grey lines lines show the elevation of the highest PPS. In areas were the PPS has been eroded, the highest remnant parts of the surface adjacent to the eroded section were used to project the original elevation of the surface. Vertical black dashed lines show the locations of major rivers (quebradas) that bisect both the Longitudinal Valley and the Coastal Cordillera en route to the Pacific Ocean.

Figure 8. N-S chronostratigraphic reconstruction of the Longitudinal Valley from northern Chile to Southern Peru. Line of section shown in Figure 1B. Dominant lithologies, unconformities, and ages compiled from previous studies (a: Alván et al., 2015; b: Tosdal et al. 1984, Quang et al. 2005, Roperch et al. 2006; c: García and Hérail 2005; d,e: Pinto et al., 2004; f: Farías et al., 2005; g: Victor et al., 2004; h,i: Sáez et al., 1999, 2012; j,k: May et al., 1999, 2005, Jordan et al., 2015; l: Evenstar et al., 2015). Stratigraphic units (grey boxes) and unconformities (red wavy lines) are shown on the right side of the figure. Abbreviations in figure; Vil. Fm = Vilama Formation, Tm. Fm = Tambores Formation, C. Fm = Calama Formation, Jal. Fm = Jalquinche Formation, Qui. Fm = Quillagua Formation and Cam A-B = Camaná Formation Unit A-B.

Figure 9. Regional sedimentation patterns over time across northern Chile and Southern Peru from the Late Oligocene to the Late Pliocene. Compiled from the chronostratigraphic reconstruction shown in Figure 8. Same lithological key as used in Figure 8.

Figure 10. Visual properties used to define characteristics of each surface showing aggradational (surfaces 1-5) and degradational (network 1 and surfaces 2 and 3) surfaces. VNIR = False colour visible near infrared satellite data where Red: Band 7 (2.1-2.35 µm), Green: Band 4 (0.75-0.9 µm), Blue: Band 2 (0.53-0.61 µm). SWIR = shortwave infrared satellite data, Hillshade = 30 m-pixel resolution digital elevation model with draped over SWIR imagery. Slope Direction = slope direction (aspect) map that illustrates the downslope direction between each pixel and its nearest neighbours indicating the dominant slope direction of surfaces over a large area,

Surface Angle = surface slope in degrees calculated from the maximum change in elevation between each 30 m pixel. Surface View = Primary ground observations of each surface described in the text.

Figure 11. (A) Mud-rich flows cover the distributive fluvial system. In Landsat VNIR and SWIR data, these flows appear white in colour (as shown in another Figure 10). (B) Aggradational Surface 1 (showing some vegetation and clear fluvial features such as bar and swale topography) superficially cuts the older, more homogenous Aggradational Surface 4. (C) An older aggradational surface exhibits a higher slope angle than the younger surface in the foreground, indicating a phase of tilting must have occurred between deposition of the two surfaces. (D) Shallow reworking of Aggradational Surface 4 by Aggradational Surface 3.

Figure 12. A compilation of cosmogenic nuclide surface exposure ages (Dunai et al. 2005, Kober et al. 2009, Evenstar et al. 2009, and this study) and the main surfaces identified across the Coastal Cordillera (CC) and the Longitudinal Valley. From oldest to youngest, these are: S5: Aggradational Surface 5 S4: Aggradational Surface 4, S3: Aggradational and Degradational Surface 3, S2: Aggradational and Degradational Surface 2, S1: Aggradational and Degradational Surface 1. Horizontal lines between data points connect samples from the same sampling site that show a variation in age. Black symbols are cosmogenic ^{3}He ages; white symbols are cosmogenic ^{21}Ne ages. Vertical dark orange bars indicate independent geochronological age constraints which overly or underlie the paleosurfaces with the pale orange bars indicating times of paleosurface formation.

Figure 13. Compilation of chronostratigraphic data from Figure 8, paleosurfaces shown in Figure 6, and the cosmogenic nuclide surface exposure ages presented in Figure 15. The main stratigraphic units shows pulses of sedimentation which are separated by unconformities that from the Aggradational Surfaces mapped in this paper and are dated using the cosmogenic nuclide exposure date in northern Chile and volcaniclastic units in southern Peru (Quang et al. 2005)

Figure 14. Summary of the main stratigraphic units in the Longitudinal Valley correlated with the paleosurfaces from each of the three region shown in Figure 6. The data are presented alongside a qualitative paleoclimate record for northern Chile from the Late Oligocene to present day (dashed line from Jordan et al. 2014; solid line based on data presented in this study); convergence rates between the Nazca and South American plates in northern Chile at 22°S (Somoza 1998); and global deep sea oxygen (dashed line) and carbon isotope (solid line) records correlated to global climatic events (Zagros et al. 2001).

Figure 15. Schematic representation of the tectono-sedimentary evolution of the Longitudinal Valley, including predominate aggradational or degradational processes through time. (A) Deposition of a series of distributary fluvial systems (the Azapa Formation) across the Longitudinal Valley and infilling parts of the Coastal Cordillera. (B) Flare up of ignimbrites across northern Chile and southern Peru. (C) Initial uplift of the Coast Cordillera restricts sedimentation of distributary fluvial systems (the El Diablo Formation) to the Longitudinal Valley. Drainage around the Bolivian Orocline is hydrologically open to the sea. The Huaylas Basin forms between the Longitudinal Valley and Precordillera at the Chile-Peru boundary (D) Quebradas Victor and Camarones incise through the Coastal Cordillera restricting deposition of distributary fluvial systems to the south of Quebrada Camarones. The Copaquilla Basin forms between the Longitudinal Valley and Precordillera at the Chile-Peru boundary. (E) Quebrada Azapa captures the Copaquilla Basin restricting further sedimentation in this basin. (F) Quebrada Tana cuts through the Coastal Cordillera restricting deposition of distributary fluvial systems to the south of the Quebrada. Areas to the east of the Altos de Pica high change from being aggradational to degradational. The Proto Rio Loa cuts through from the Calama Basin to the Quillagua Llamara Basin. At the end of this period, Quebrada Lluta captures the Huaylas Basin restricting further sedimentation in this basin. (G) The Rio Loa cuts through the Coastal Cordillera to the Pacific Ocean. The last large-scale distributary fluvial systems are deposited across the region before the region reverts to the present day hyperarid conditions.

(H) Modern day hyperarid conditions see the telescoping of distributary fluvial systems into the Longitudinal Valley.

Table 1. ^{3}He and ^{21}Ne data and apparent surface exposure ages. Exposure ages are calculated using Lal (1991) modified by Stone (2000) scaling factors.

Table 2. Physical properties of each defined paleosurface.

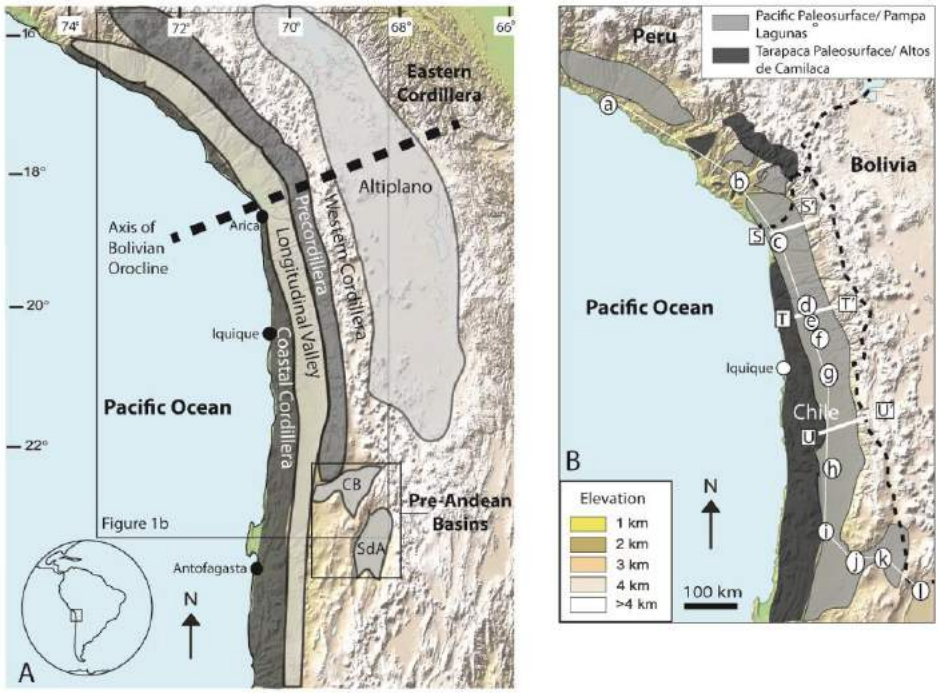

Figure 1

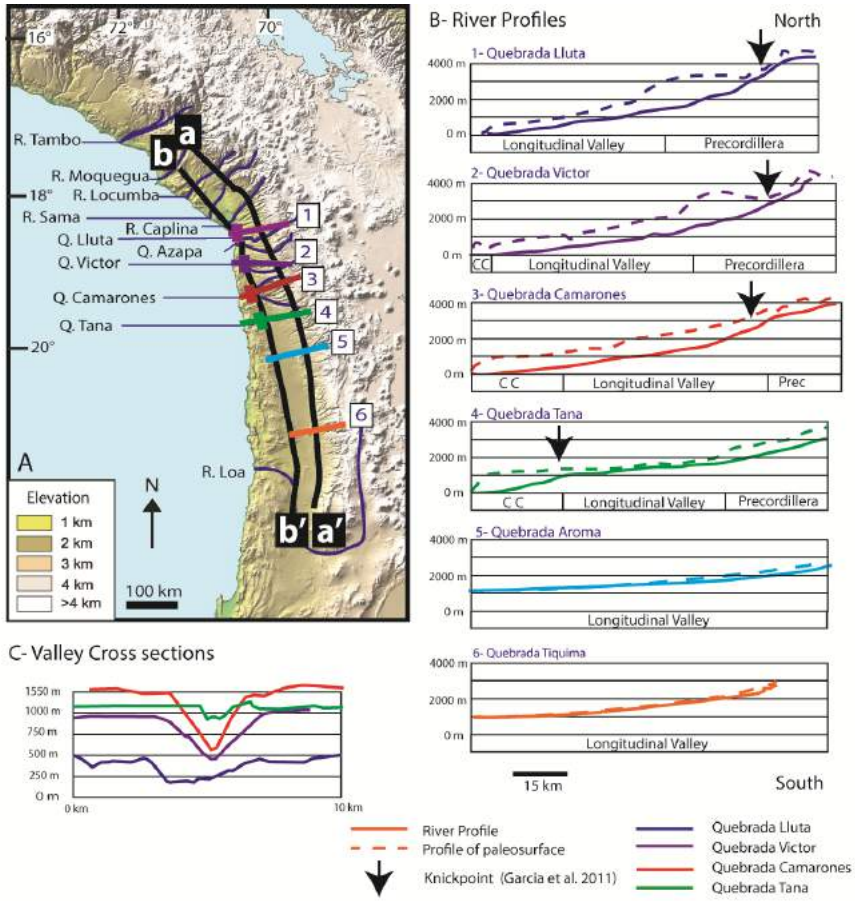

Figure 2

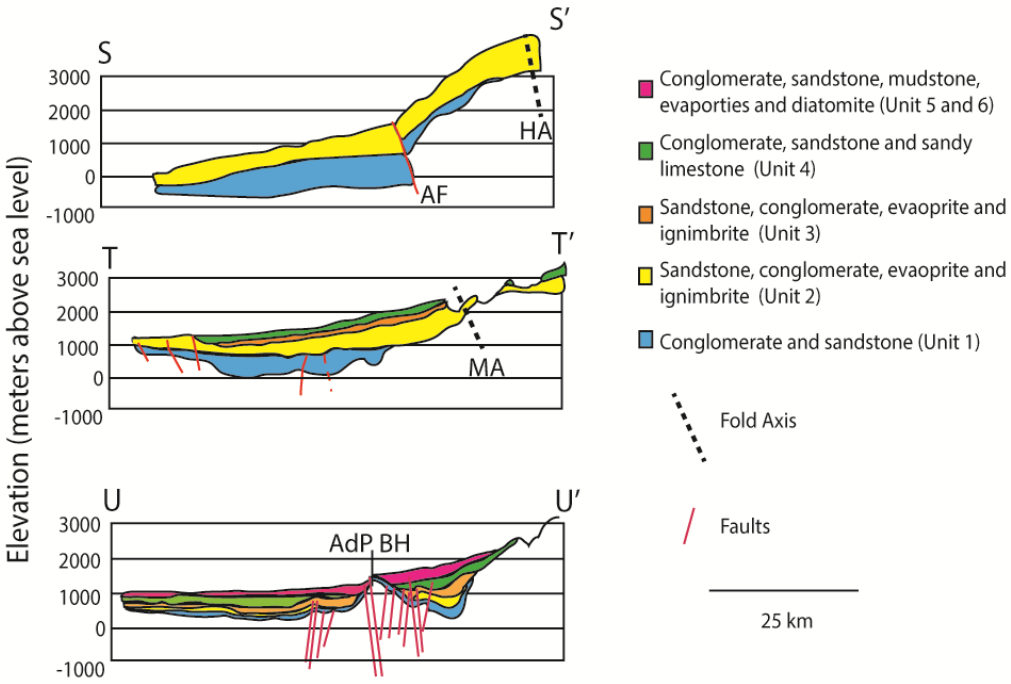

Figure 3

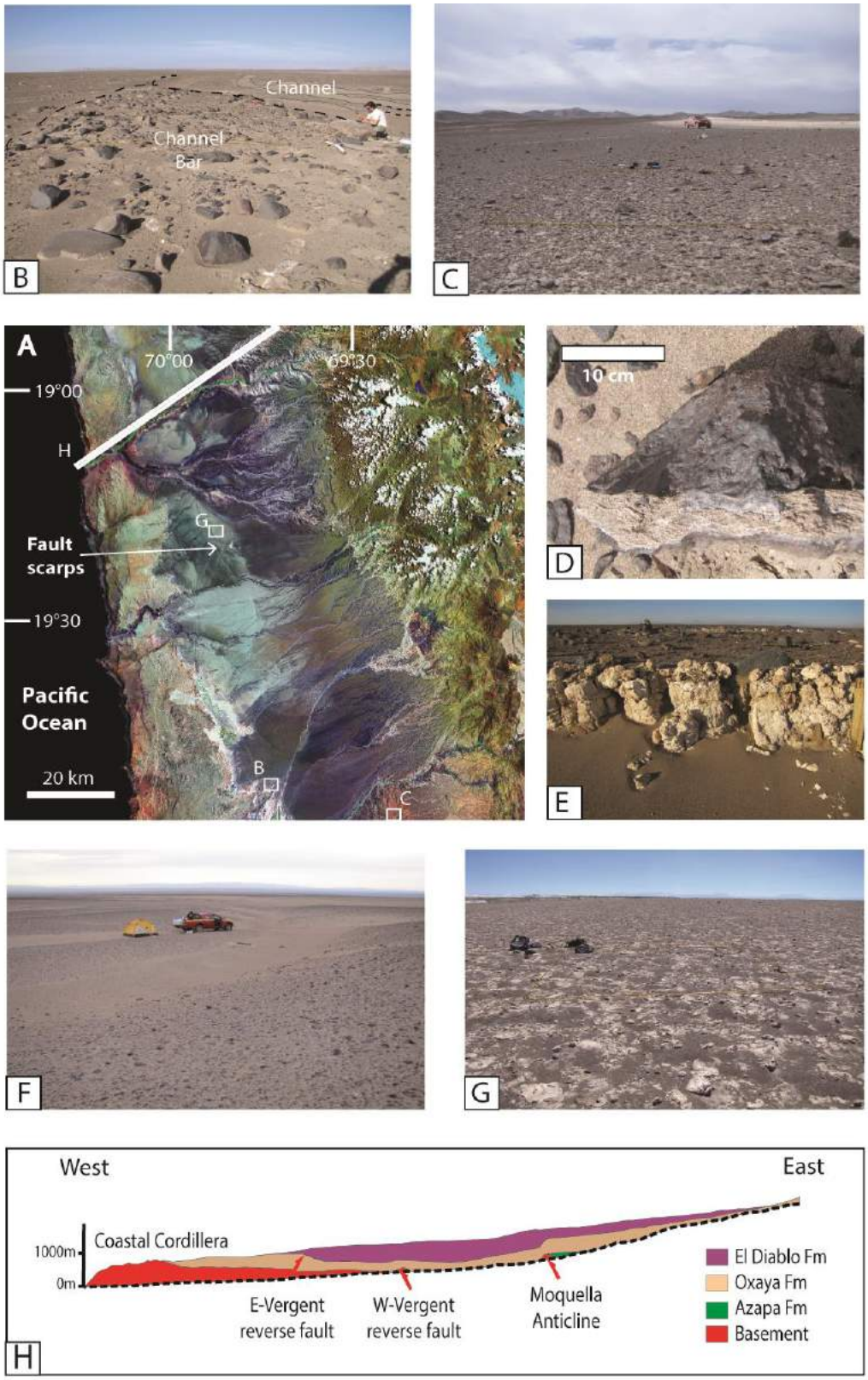

Figure 4

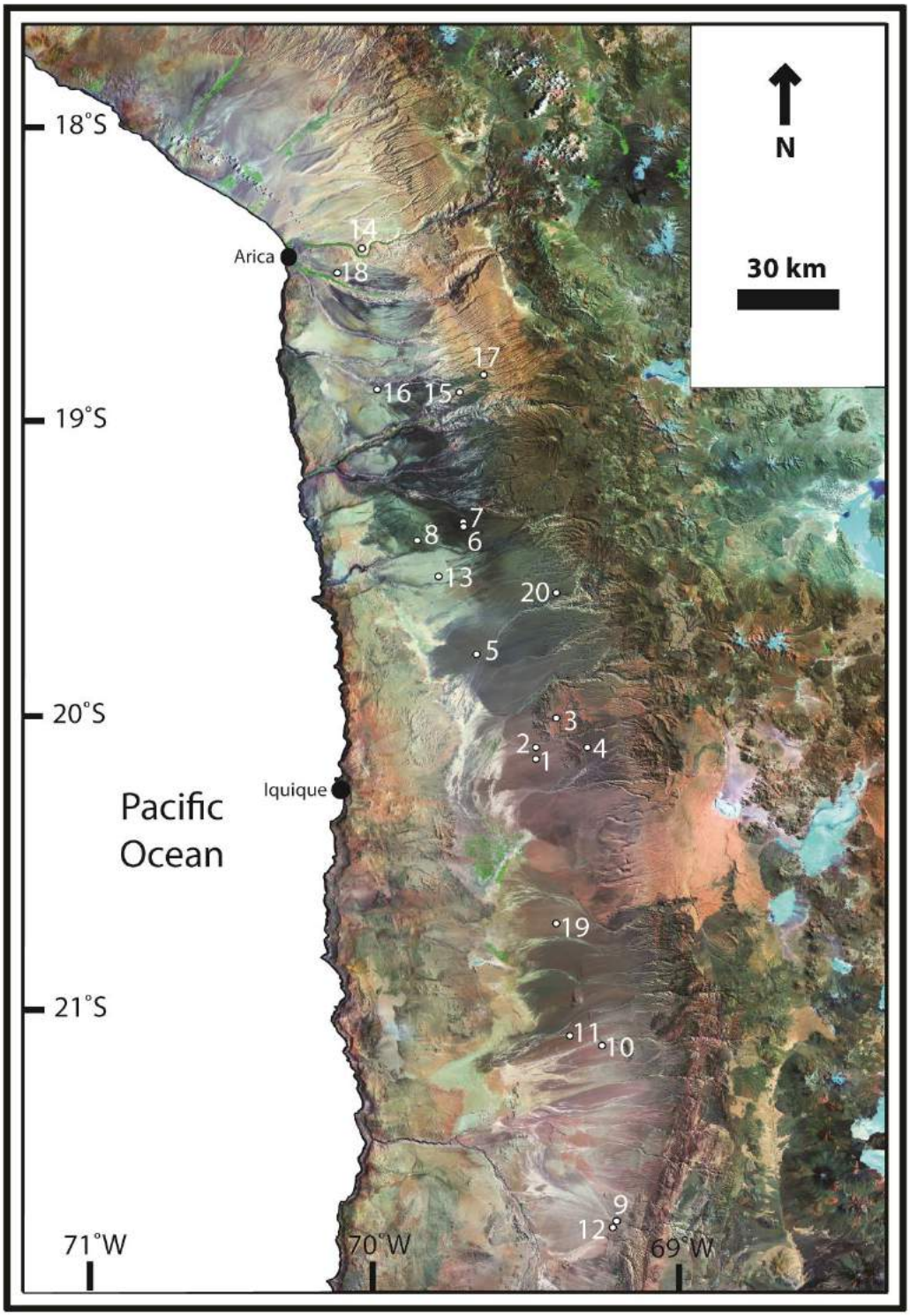

Figure 5

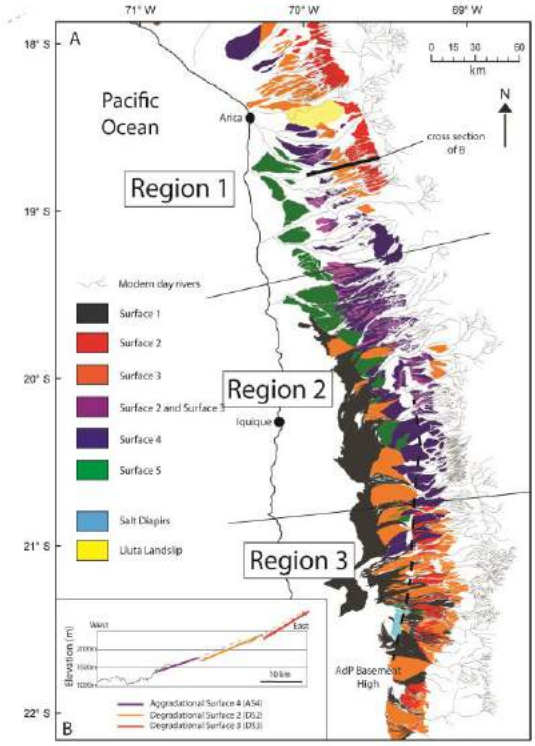

Figure 6

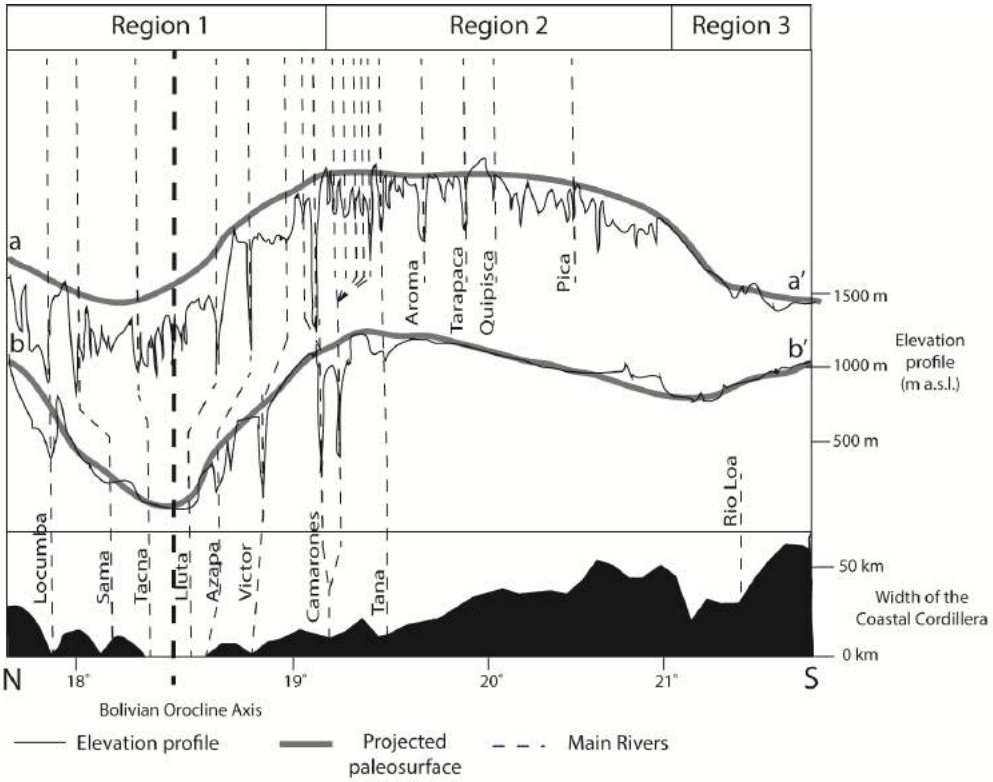

Figure 7

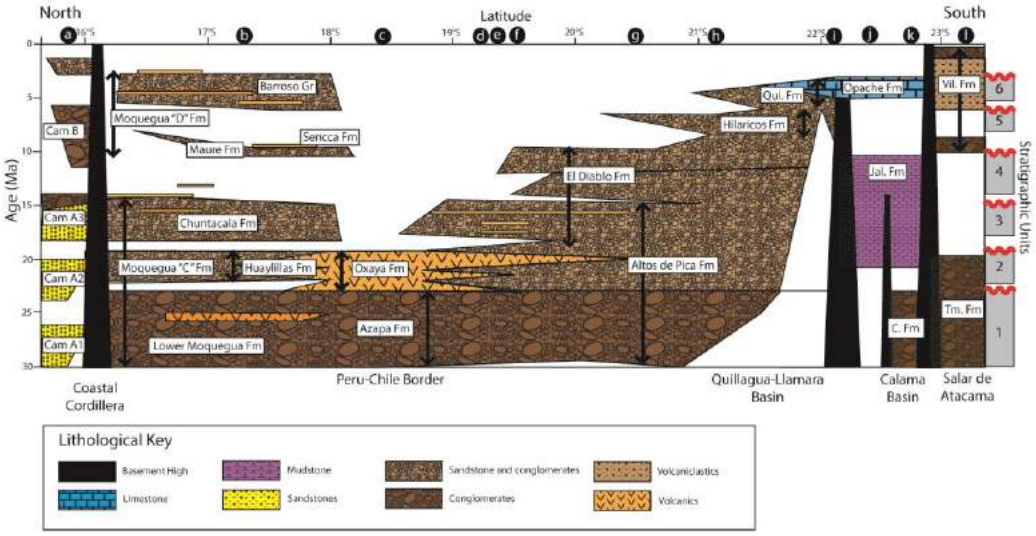

Figure 8

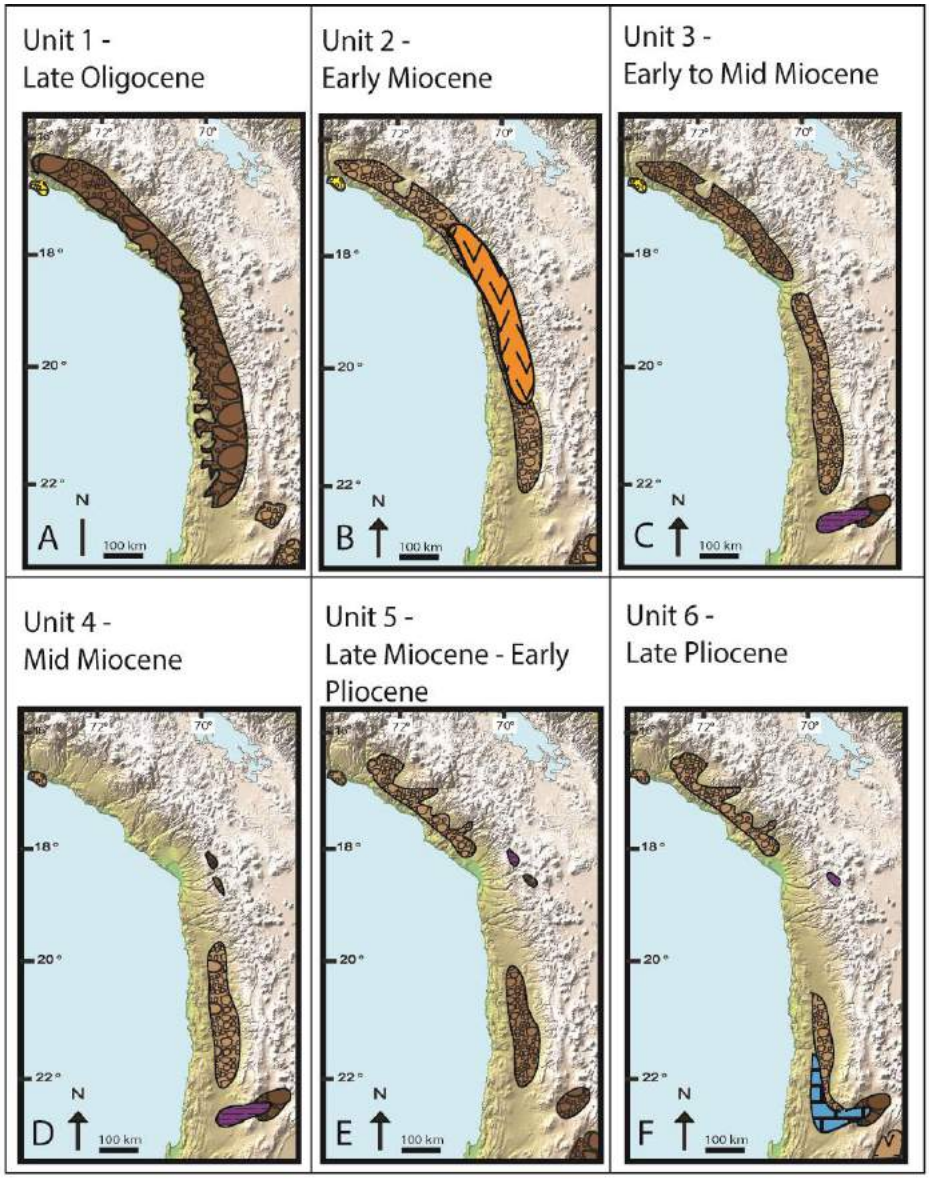

Figure 9

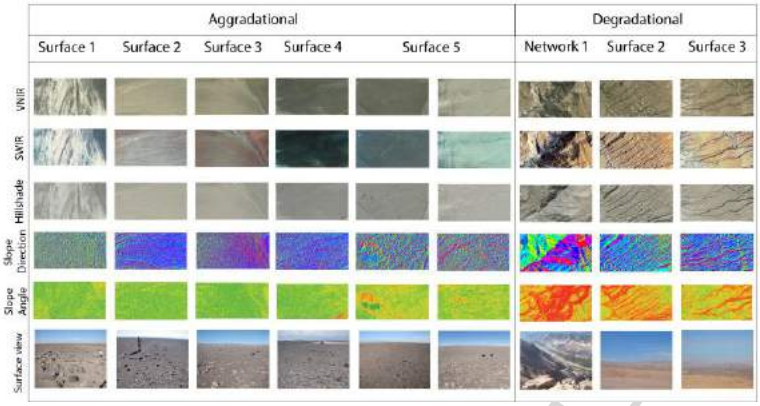

Figure 10

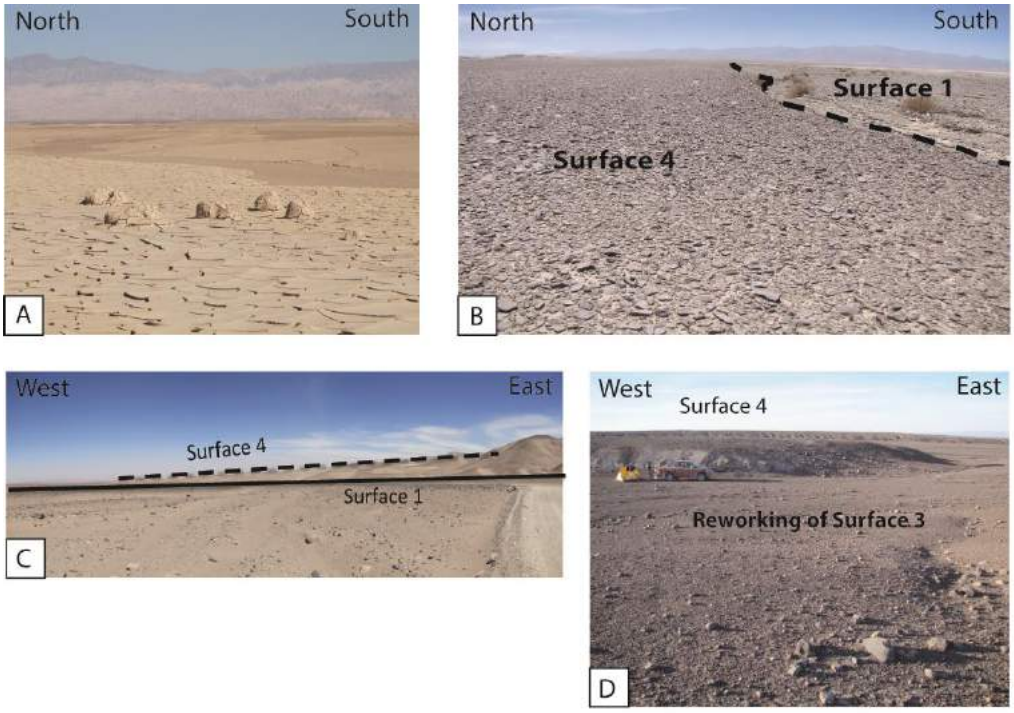

Figure 11

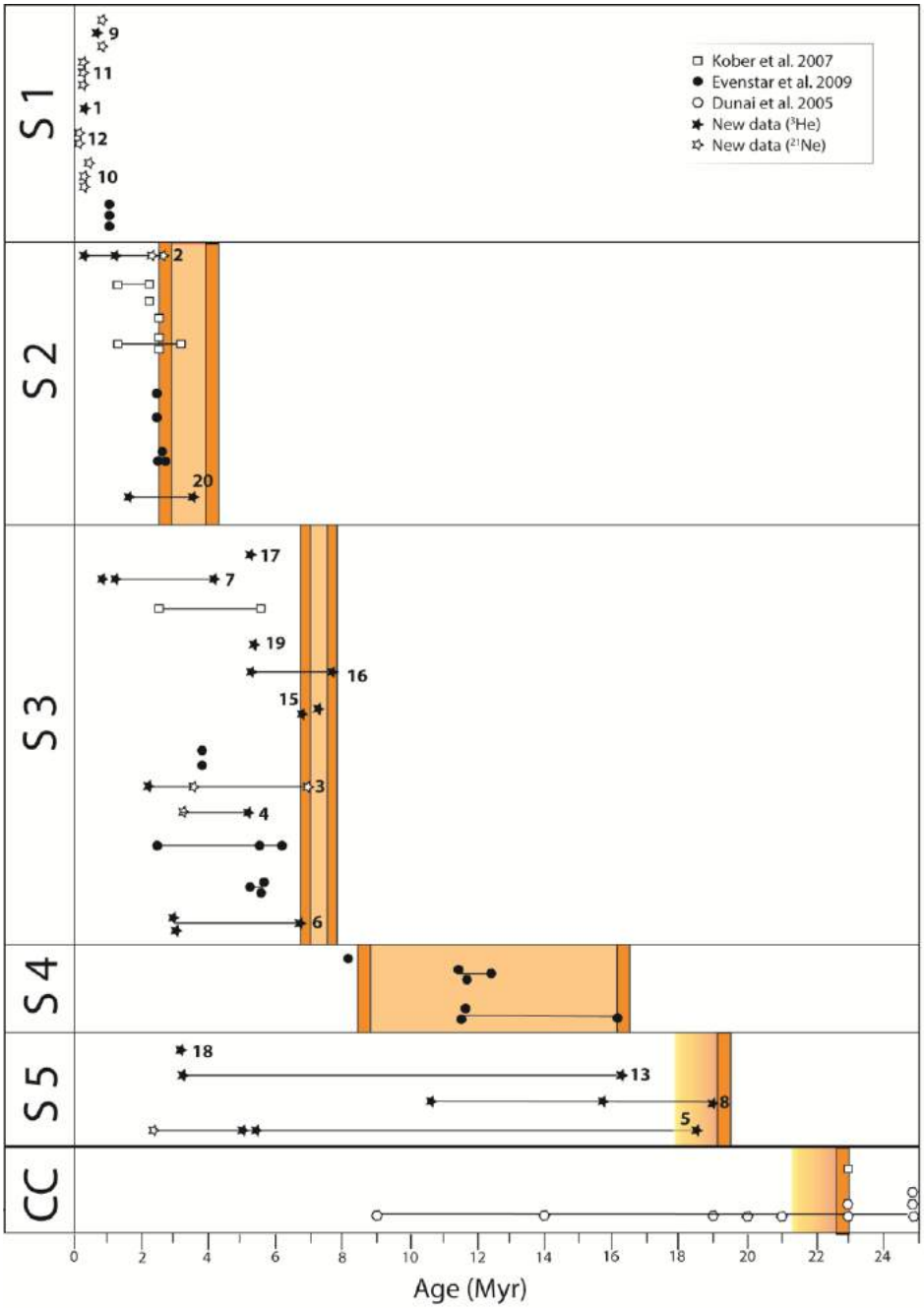

Figure 12

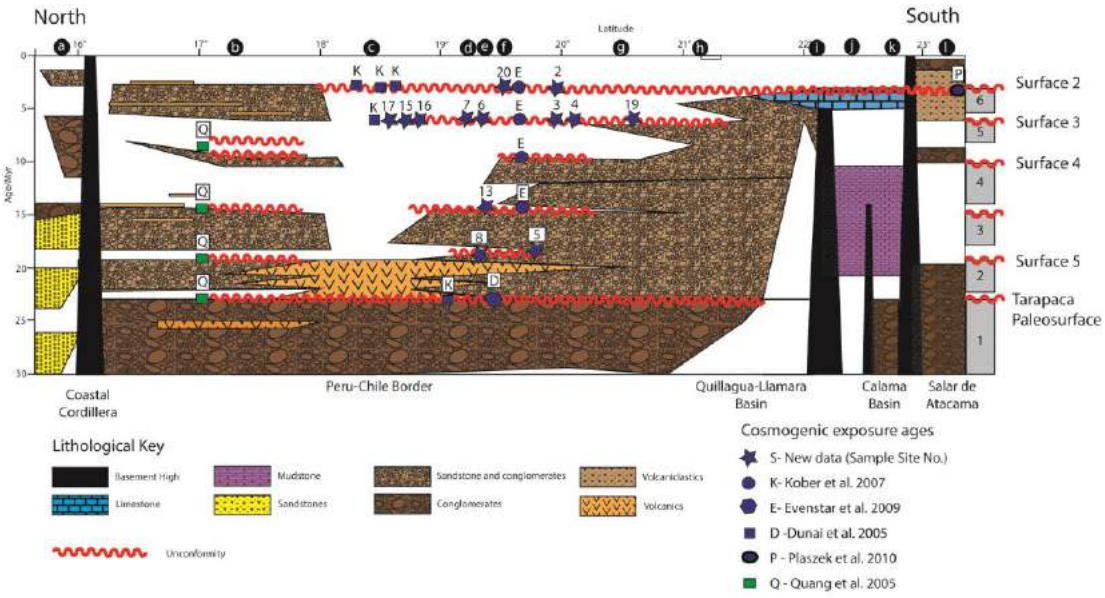

Figure 13

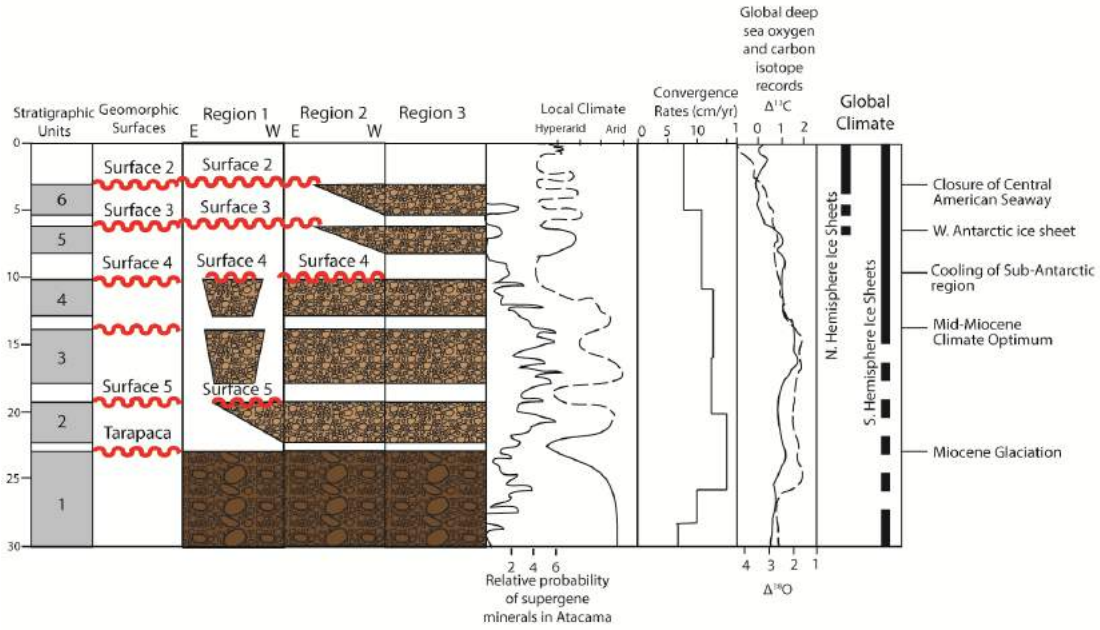

Figure 14

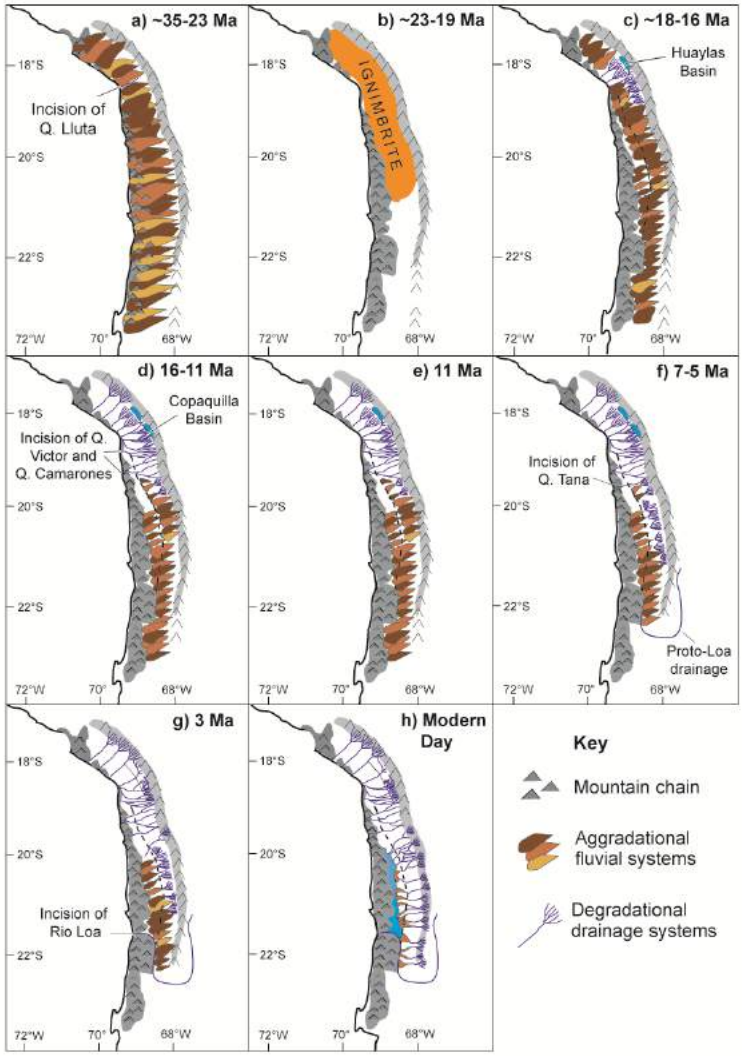

Figure 15

Table 1

Surface	Sample Site	Sample Name	Latitude (decimal degrees)	Lonitude (decimal degrees)	Elevation (m)	Isotope	Mineral	Density of rock (g cm^3)	^{21}Ne or ^{3}He (10^7 at. g)	^{21}Ne or ^{3}He Error ± 1σ (10^7 at. g)	Scaling factor	Apparent Exposure Age (Ma)	Error ± 1σ (Ma)
Surface 1	1	Day 01-04	-20.138944	-69.488389	1316	He	Amphibole	2.86	6.64	0.13	Lm	0.29	0.02
	9	Sample 1	-21.724806	-69.237972	1676	Ne	Quartz	2.74	3.87	0.37	Lm	0.95	0.09
		Sample 2	-21.724806	-69.237972	1676	He	Amphibole	2.86	19.77	0.77	Lm	0.71	0.03
		Sample 3	-21.724806	-69.237972	1676	Ne	Quartz	2.74	3.79	0.25	Lm	0.93	0.06
	10	Sample 7	-21.704056	-69.209444	1438	Ne	Quartz	2.74	0.95	0.15	Lm	0.22	0.03

		Sample 8	-21.704056	-69.209444	1438	Ne	Quartz	2.74	0.42	0.13	Lm	0.09	0.03
		Sample 9	-21.704056	-69.209444	1438	Ne	Quartz	2.74	1.11	0.20	Lm	0.25	0.05
	11	Sample 10	-21.101222	-69.2575	1065	Ne	Quartz	2.74	0.58	0.08	Lm	0.16	0.02
		Sample 12	-21.101222	-69.2575	1065	Ne	Quartz	2.74	0.69	0.08	Lm	0.19	0.02
	12	Sample 13	-21.078944	-69.364833	1573	Ne	Quartz	2.74	0.14	0.02	Lm	0.05	0
Surface 2	2	Day 01-05	-20.101167	-69.491222	1380	He	Pyroxene/Olivine	3.2	3.23	0.49	Lm	0.14	0.02
		Day 02-01	-20.101167	-69.491222	1380	Ne	Quartz	2.74	7.50	0.44	Lm	2.34	0.13
		Day 02-02	-20.101167	-69.491222	1380	He	Olivine	3.2	25.90	0.88	Lm	1.15	0.04
		Day 02-03	-20.101167	-69.491222	1380	Ne	Quartz	2.74	7.87	0.64	Lm	2.52	0.19
	20	21/10	-	-	1172	He	Pyroxene	2.89	65.9	1.2	Lm	3.58	0.07

		20/10	19.578942 - 19.578942	69.872967 - 69.872967	1172	He	Pyroxene	2.89	1 32.20	0 0.70	Lm	1.7	0.04
Surface 3	3	Day 02-10	- 19.987111	- 69.433611	1943	Ne	Quartz	2.74	16.74	0.99	Lm	3.59	0.14
		Day 02-11	- 19.987111	- 69.433611	1943	He	Pyroxene	2.89	63.88	2.57	Lm	1.95	0.08
		Day 02-12	- 19.987111	- 69.433611	1943	Ne	Quartz	2.74	33.10	1.34	Lm	7.04	0.32
	4	Day 03-01	- 20.108222	- 69.311722	2233	He	Amphibole	2.86	225.28	6.40	Lm	5.62	0.18
		Day 3-03	- 20.108222	- 69.311722	2233	Ne	Quartz	2.74	19.91	0.76	Lm	3.31	0.13
	6	Day 4-02	- 19.340944	-69.728	1607	He	Pyroxene	2.89	74.48	2.33	Lm	2.93	0.09
		Day 04-03	- 19.340944	-69.728	1607	He	Pyroxene	2.89	91.10	1.30	Lm	3.62	**0.05**
		Day 4-04	- 19.3409	-69.728	1607	He	Pyroxene	2.89	167.12	3.65	Lm	6.95	0.14

7	Day 04-10	-44 19.336722	-69.729611	1604	He	Pyroxene	2.89	24.27	1.05	Lm	0.93	0.04
	Day 04-11	-19.336722	-69.729611	1604	He	Pyroxene	2.89	31.18	1.19	Lm	1.2	0.04
	Day 4-12	-19.336722	-69.729611	1604	He	Pyroxene	2.89	104.68	2.24	Lm	4.22	0.07
15	10/21	-18.886583	-69.699056	2282	He	Pyroxene	2.89	269.89	4.73	Lm	7.15	0.14
	08/21	-18.886583	-69.699056	2282	He	Pyroxene	2.89	246.53	4.29	Lm	6.49	0.12
16	23/21	-18.905639	-69.954583	1443	He	Pyroxene	2.89	141.41	2.52	Lm	5.26	0.12
	24/21	-18.905639	-69.954583	1443	He	Pyroxene	2.89	164.80	2.84	Lm	7.9	0.15
17	02/21	-18.852694	-69.657167	2550	He	Pyroxene	2.89	235.00	4.04	Lm	5.13	0.09
19	10/10	-20.704083	-69.420833	1084	He	Pyroxene	2.89	90.19	1.97	Lm	5.26	0.02

Surface 5	5	Day 03-10	-19.786306	-69.682	1289	He	Pyroxene	2.89	107.80	2.77	Lm	5.52	0.13
		Day 3 -11	-19.786306	-69.682	1289	He	Pyroxene	2.89	102.49	2.48	Lm	5.24	0.12
		Day 3-12	-19.786306	-69.682	1289	Ne	Quartz	2.74	7.24	0.62	Lm	2.3	0.21
		01/02	-19.786306	-69.682	1289	He	Pyroxene	2.89	298.96	3.20	Lm	18.41	0.25
	8	Day 05-01	-19.397833	-69.880306	1256	He	Pyroxene	2.89	194.23	4.67	Lm	11.08	0.27
		Day 05-02	-19.397833	-69.880306	1256	He	Pyroxene	2.74	310.26	8.23	Lm	20.17	0.65
		Day 5 -03	-19.397833	-69.880306	1256	He	Pyroxene	2.89	269.16	6.18	Lm	16.6	0.42
	13	01/12	-19.522111	-69.808333	1312	He	Pyroxene	2.89	277.15	5.20	Lm	16.29	0.4
		02/12	-19.522111	-69.808333	1312	He	Pyroxene	2.89	65.40	1.50	Lm	3.19	0.04
	18	07/18	-	-	771	He	Pyroxene	2.89	41.2	0.7	Lm	3.08	0.06

			18.503528	70.143306					9	2					
Lluta	14	06/16	-18.389944	-70.071806	1025	He	Pyroxene	2.89	38.80	0.77	Lm	2.36	0.05		
Collapse		09/16	-18.389944	-70.071806	1025	He	Pyroxene	2.89	42.50	0.95	Lm	2.6	0.06		

Table 2

Relative age of surface	Type of Surface	Drainge type	Angle of surface	Digital Elevation Model (DEM)	Google Earth Colour	Sedimentary features	LANDSAT COLOUR	Slope Direction
Surface 1	Degradational (DS1)	Dendretic drainage	0-5°	N/A	N/A	Inisional drainage	N/A	None
	Aggradational (AS1)	Fans	0-5	Smooth	White/ cream	Clear fluvial features	Pale blue to yellow	None
Surface 2	Degradational (DS2)	Parallel drainage	0-5°	N/A	Orange/ cream brown	Inisional drainage	Orange to pale pink	West
	Aggradational (AS2)	Fans	0-5°	Smooth	Grey/ pink brown	Clear fluvial and alluvial features	Dark red to red brown	None
Surface 3	Degradational (DS3) (North of 19°S)	Dendretic drainage	2.5-7.5°	N/A	Pink/ Orange/ Cream	Inisional drainage	Pale blue/ white/ orange	West
	Degradational (DS3) (South of 19°S)	Dendretic drainage	2.5-7.5°	N/A	Pink/ yellow grey	Inisional drainage	Dark Blue grey to dark olive green	West
	Aggradational (AS3)	Fans	2.5-7.5°	Smooth	Dark brown to pale red	Clear alluvial features	Dark blue grey to dark red	Slope follows fan shape
Surface 2 and 3 (Reworking of **Surface 4)**	Aggradational and degradational	Fluvial	5-7.5°	Smooth	Grayish blue	Clear fluvial features	Blue grey	South West

Surface 4	Aggradational (AS4)	Unknown	5-7.5°	Smooth	Dark brown to orange in the north Red brown on the south	No clear depositional features	Very dark brown/blue and green in the north to dark red in the south	South West
Surface 5	Aggradational (AS5)	Unknown	0-7.5° (North of 19°30') 5-15° (South of 19°30')	Rough	Yellow ream colour in north and dark red brown in the south	No clear depositional features, clear tectonics fractures across the surface.	Pale green in norht to dark brown/ red in south	North (North of 19°30') South (South of 19°30')